Journal of Statistical Physics, Vol. 72, Nos. 5/6, 1993

Trapping, Percolation, and Anomalous Diffusion of Particles in a Two-Dimensional Random Field

Marco Avellaneda,[1] Frank Elliott, Jr.,[2] and Christopher Apelian[1]

Received October 12, 1992; final April 1, 1993

We analyze from first principles the advection of particles in a velocity field with Hamiltonian $H(x, y) = \bar{V}_1 y - \bar{V}_2 x + W_1(y) - W_2(x)$, where W_i, $i = 1, 2$, are random functions with stationary, independent increments. In the absence of molecular diffusion, the particle dynamics are very sensitive to the streamline topology, which depends on the mean-to-fluctuations ratio $\rho = \max(|\bar{V}_1|/\bar{U}; |\bar{V}_2|/\bar{U})$, with $\bar{U} = \langle |W_1'|^2 \rangle^{1/2} =$ rms fluctuations. Remarkably, the model is exactly solvable for $\rho \geqslant 1$ and well suited for Monte Carlo simulations for all ρ, providing a nice setting for studying seminumerically the influence of streamline topology on large-scale transport. First, we consider the statistics of streamlines for $\rho = 0$, deriving power laws for $p_{nc}(L)$ and $\langle \lambda(L) \rangle$, which are, respectively, the escape probability and the length of escaping trajectories for a box of size L, $L \gg 1$. We also obtain a characterization of the "statistical topography" of the Hamiltonian H. Second, we study the large-scale transport of advected particles with $\rho > 0$. For $0 < \rho < 1$, a fraction of particles is trapped in closed field lines and another fraction undergoes unbounded motions; while for $\rho \geqslant 1$ all particles evolve in open streamlines. The fluctuations of the free particle positions about their mean is studied in terms of the normalized variables $t^{-\nu/2}[x(t) - \langle x(t) \rangle]$ and $t^{-\nu/2}[y(t) - \langle y(t) \rangle]$. The large-scale motions are shown to be either Fickian ($\nu = 1$), or superdiffusive ($\nu = 3/2$) with a non-Gaussian coarse-grained probability, according to the direction of the mean velocity relative to the underlying lattice. These results are obtained analytically for $\rho \geqslant 1$ and extended to the regime $0 < \rho < 1$ by Monte Carlo simulations. Moreover, we show that the effective diffusivity blows up for resonant values of $(\bar{V}_1, \bar{V}_2)$ for which stagnation regions in the flow exist. We compare the results with existing predictions on the topology of streamlines

[1] Courant Institute of Mathematical Sciences, New York, New York 10012.

[2] Program in Computational and Applied Mathematics, Princeton University, Princeton, New Jersey 08544.

0022-4715/93/0900-1227$07.00/0

based on percolation theory, as well as with mean-field calculations of effective diffusivities. The simulations are carried out with a CM 200 massively parallel computer with 8192 SIMD processors.

KEY WORDS: Trapping; percolation; superdiffusion.

1. INTRODUCTION AND STATEMENT OF THE RESULTS

Investigations of large-scale transport in heterogeneous media often involve monitoring the evolution of a passive scalar in a random, incompressible velocity field described by the mass-balance equation

$$\frac{\partial C(\mathbf{r}, t)}{\partial t} + \mathbf{V}(\mathbf{r}) \cdot \nabla C(\mathbf{r}, t) = 0 \tag{1}$$

For instance, in hydrological modeling of flow in porous media, $\mathbf{V}(\mathbf{r})$ represents the Darcy velocity of the saturating fluid, and $C(\mathbf{r}, t)$ denotes the concentration of a solute spreading in the solid/fluid aggregate. The stochasticity of $\mathbf{V}(\mathbf{r})$ models reservoir heterogeneities on a field scale. For a given initial concentration $C(\mathbf{r}, 0) = C_0(\mathbf{r})$, this equation can be integrated using its characteristics,

$$\frac{d\mathbf{r}(t)}{dt} = \mathbf{V}(\mathbf{r}(t)) \tag{2}$$

which represent the equations of motion of solute fluid elements, or particles. Accordingly, the concentration at time τ and location $\mathbf{r}$ is given by

$$C(\mathbf{r}, \tau) = C_0(\mathbf{r}(0))$$

where $\mathbf{r}(t)$, $0 \leqslant t \leqslant \tau$, is the particle trajectory satisfying $\mathbf{r}(\tau) = \mathbf{r}$.

The primary importance of this equation is to predict the long-time/large-scale evolution of $C(\mathbf{r}, t)$ based on the input of the reservoir properties through the statistical distribution of $\mathbf{V}(\mathbf{r})$. For instance, an initial datum $C_0(\mathbf{r}) = H(\mathbf{r} \cdot \mathbf{n})$, where H is a Heaviside step function and $\mathbf{n}$ is a unit vector, corresponds to a "piston-flow" model in which an initial half-space of solute, with a planar interface orthogonal to $\mathbf{n}$, evolves into a wrinkled front permeating the medium. The mean position of the front at time $t > 0$ will be associated with the average $\langle \mathbf{r}(t) \rangle$ of particles originating at the interface at time $t = 0$. The Lagrangian standard deviation

$$\langle |(\mathbf{r}(t) - \langle \mathbf{r}(t) \rangle) \cdot \mathbf{n}|^2 \rangle^{1/2}$$

characterizes the width of the spreading front about its mean position, or *mixing length*, a fundamental quantity in solute transport (see, e.g., ref. 1).

Fick's law of diffusion states that

$$\langle |\mathbf{r}(t) - \langle \mathbf{r}(t) \rangle|^2 \rangle \propto D^* t, \qquad t \gg 1$$

and

$$\frac{1}{\sqrt{t}} [\mathbf{r}(t) - \langle \mathbf{r}(t) \rangle] \sim \text{Gaussian}, \qquad t \gg 1$$

where D^* is an effective long-time diffusion coefficient. While Fick's law is valid in many cases, it has been recognized for some time that the long-time behavior of stochastic transport is far from universal. In fact, certain statistical features of the velocity $\mathbf{V}$ give rise to anomalous, or non-Fickian, transport, with

$$\langle |\mathbf{r}(t) - \langle \mathbf{r}(t) \rangle|^2 \rangle \propto t^{\nu}, \qquad \nu \neq 1, \quad t \gg 1$$

and with a non-Gaussian asymptotic distribution of the fluctuations $t^{-\nu/2}[\mathbf{r}(t) - \langle \mathbf{r}(t) \rangle]$, in which "memory" effects in the Lagrangian history are important. Mechanisms linked to anomalous diffusion in the literature include, on the one hand, long-range spatial correlations of the velocity as a source for superdiffusion ($\nu > 1$),[2-4] as well as, in the case of diffusionless two-dimensional transport, the "trapping" of advected particles along closed streamlines, associated with subdiffusive behavior ($\nu < 1$).[2] First-principles calculations of D^* or of the exponent ν require solving the equations of motion (2) to some extent and are consequently very difficult. Most work in this area has been based on applying one form or another of statistical closure to (1) or (2), i.e., in treating the long-time asymptotic distribution of advected particles as a "quasiequilibrium" state, described in terms of low-order statistics of the velocity field. These procedures, known as renormalized perturbation theories, include, most notably, the direct interaction approximation (DIA),[5] introduced by R. Kraichnan in the late 1950s as a general tool for studying turbulent transport.[6] Renormalization theories can capture "universal" features of stochastic transport and often predict accurate quantitative values for the effective diffusivity, etc. On the other hand, since these theories are based on a mean-field approximation, namely the hypothesis of quasiequilibrium of the Lagrangian particles with respect to the random environment for $t \gg 1$, the question of how well they represent the true dynamics poses itself, especially for systems in which velocity fluctuations are important over a wide dynamical range. For instance, in the absence of molecular diffusion, the random velocity can trap the particle in a closed streamline or, to the contrary, transport it over

a long distance over a long or open streamline. All this can lead to complicated statistics for the dynamics, the study of which lies beyond the scope of renormalized perturbation theories. Exactly solvable models have been proposed recently, in the context of stratified random flows, as an attempt to understand better the issue of anomalous transport.[7–9] In a similar spirit, the properties of large-scale transport for two- or three-dimensional velocities with complex Lagrangian structure should be explored through simple models which, if not exactly solvable, are to some extent amenable to first-principles calculations and well suited for Monte Carlo simulation.

In this paper we study analytically and numerically a two-dimensional model of dispersion in a random incompressible flow which has several interesting features in the long-time limit. In our model, the velocity takes values on a discrete set, according to the position of the particle relative to a random grid in the plane. The Lagrangian equations that we consider have the form

$$\begin{cases} \dfrac{dx(t)}{dt} = \bar{V}_1 + U_1(y(t)) \\ \dfrac{dy(t)}{dt} = \bar{V}_2 + U_2(x(t)) \end{cases} \tag{3}$$

where $U_1(y) = \pm\bar{U}$ and $U_2(x) = \pm\bar{U}$. Here $\bar{U}$ is a positive constant; the functions $U_1(y)$ and $U_2(x)$ are piecewise constant over intervals of random, exponentially distributed lengths. The vector $\bar{\mathbf{V}} = (\bar{V}_1, \bar{V}_2)$ represents the uniform mean velocity and $\mathbf{U}(x, y) = (U_1(y), U_2(x))$ represents the fluctuating velocity which would arise, say, from pressure fluctuations in the underlying porous medium. Thus, in this discrete model, the fluctuating component of the velocity points in one of four directions, $\mathbf{U} = \bar{U}(\pm 1, \pm 1)$, while the mean velocity is allowed to vary continuously. A primary focus of the present study is the assessment of the influence of the mean-to-fluctuations ratio $|\bar{V}|/\bar{U}$ on large-scale transport, and in particular on the anomalous effects which arise as the amplitude and direction of $\bar{V}$ are varied, with $\mathbf{U}(x, y)$ held fixed.

The system (3) has a (random) Hamiltonian

$$\begin{aligned} H(x, y) &= \bar{V}_1 y - \bar{V}_2 x + \int_0^y U_1(y')\, dy' - \int_0^x U_2(x')\, dx' \\ &\equiv \bar{V}_1 y - \bar{V}_2 x + W_1(y) - W_2(x) \end{aligned} \tag{4}$$

Because of our assumptions, the functions W_i in (4) behave statistically like continuous-time Brownian walks at large distances. This model is a special case of a larger class of random Hamiltonian flows with

$$H(x, y) = \bar{V}_1 y - \bar{V}_2 x + \sum_{j=1}^{N} b_j W_j(\mathbf{r} \cdot \mathbf{n}_j) \tag{5}$$

where $W_j(z)$, $j = 1,..., N$, are independent, two-sided $(-\infty < z < +\infty)$, continuous-time random walks, b_j are constant coefficients, and $\mathbf{n}_j$ are vectors in 2D Euclidean space. For simplicity we shall discuss here only (4), which is the simplest example of (5) which exhibits nonlinear coupling of the x and y components and is therefore truly two dimensional. A closely related model was analyzed in the case $\bar{\mathbf{V}} = 0$, with nonzero molecular diffusion, by Redner[10] and Bouchaud *et al.*,[11] using mean-field methods.

This paper concerns two related questions. First, we study the *statistical topography*, i.e., the statistical properties of the isolines of the random Hamiltonian (4), which are the streamlines of Eq. (3). Particular attention is devoted to the question of "trapping" and "percolation" of streamlines, according to the values of the mean-to-fluctuations ratio $|\bar{\mathbf{V}}|/|\bar{U}|$. The fractal dimension of long streamlines is calculated, as well as the probability that a streamline diameter exceeds a given length. Second, we study the *long-time transport of particles under a nonzero mean velocity*, focusing on the dispersion of particles from their mean position. We compute the diffusion coefficients as a function of the mean-to-fluctuations ratio and show that certain resonant velocities give rise to superdiffusive transport in some cases and to very large values of the effective diffusivities in others. In the former cases, a superdiffusive exponent $\nu = 3/2$ is found and the effective one-particle Green function (propagator) is characterized as well. These questions are analyzed theoretically in the regime $|\bar{V}| \geqslant \bar{U}$ as well as by Monte Carlo simulations in all cases. The simulations are done with a Connection Machine 200 with 2–8K SIMD processors. Each processor is assigned an independent realization of the velocity of size (up to) $L \approx 2^{15}$. We compare the analytical results available for the regime $|\bar{\mathbf{V}}| > \bar{U}$ with simulations and obtain agreement up to several significant digits, thus validating the computer simulations. The numerics are then used to explore the regime of strong fluctuations $|\bar{\mathbf{V}}| < \bar{U}$. The large number of realizations, as well as the large system size, ensure a high accuracy of the numerical results. We describe hereafter the results of this study in more detail.

The first results concern the structure of the streamlines of the Lagrangian equation. The present model exhibits two transitions as the parameter

$$\rho = \max\left(\frac{|\bar{V}_1|}{\bar{U}}, \frac{|\bar{V}_2|}{\bar{U}}\right)$$

is varied. For $\rho = 0$ (purely fluctuating velocity) all streamlines are closed and finite. For $0 < \rho < 1$ (weak mean-to-fluctuations ratio) the fraction of

open streamlines is positive but less than 1, while for $\rho \geqslant 1$ (strong mean-to-fluctuations ratio), all streamlines are open, except for the case $|\bar{V}_1| = |\bar{V}_2| = \bar{U}$, in which the mean flow has a finite probability ($p = 0.25$) of exactly canceling the fluctuations, producing an array of "pockets" in which particles are stagnant. We shall refer to the case $0 < \rho < 1$ as the *subcritical* regime, the cases $\rho > 1$, or $\rho = 1$, with $|\bar{V}_1| \neq |\bar{V}_2|$ as the *supercritical* regime, and the case $\rho = 1$, $|\bar{V}_1| = |\bar{V}_2|$ as the *diagonal-resonant* regime (Fig. 1). Despite the simplicity of the velocity field, the random streamline pattern for a given realization is quite complex. The percolation properties of streamlines are studied quantitatively. For $\rho = 0$, we find that streamlines with arbitrarily large diameter can occur, and that the probability that a randomly chosen streamline exceeds a diameter $L \gg 1$ scales like

$$p_{nc}(L) \sim L^{-\alpha}, \qquad \alpha = 0.21 \pm 0.017$$

The expectation value of the length $\lambda(L)$ of a streamline exceeding a diameter L is shown to scale like

$$\langle \lambda(L) \rangle \approx L^{\gamma}, \qquad \gamma = 1.28 \pm 0.015$$

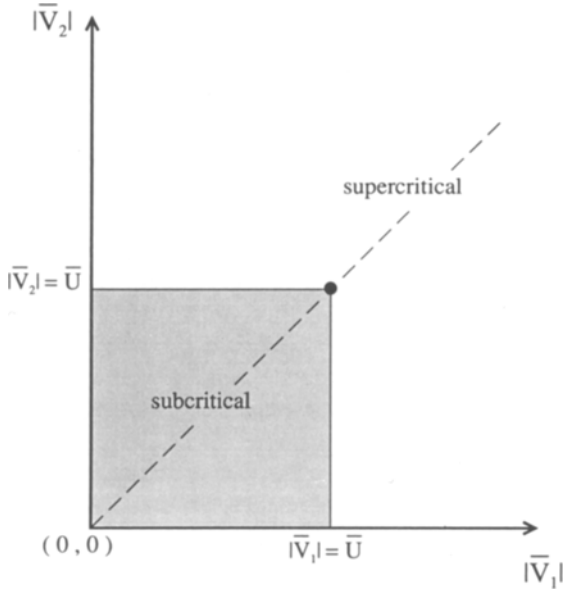

Fig. 1. The different dynamical regimes are shown in the $(|\bar{V}_1|, |\bar{V}_2|)$ plane. The gray box corresponds to the subcritical region, where $\rho = \max(|\bar{V}_1|/\bar{U}, |\bar{V}_2|/\bar{U}) < 1$. The exterioe of the box corresponds to the supercritical regime $\rho \geqslant 1$. The coordinate axes $(|\bar{V}_1| \cdot |\bar{V}_2| = 0)$ correspond to velocities giving rise to superdiffusion in the longitudinal direction ("parallel resonance"). The corner of the box indicated with a black dot indicates the "diagonal-resonant" point $|\bar{V}_1| = |\bar{V}_2| = \bar{U}$ where the effective diffusivities blow up.

This scaling law for $\lambda(L)$ appears to hold even *without* ensemble averaging, so that a randomly chosen streamline with diameter larger than L will satisfy

$$\frac{\log \lambda(L)}{\log L} \approx 1.28 \pm 0.015$$

with probability 1. In other words, $\log \lambda(L)/\log L$ is a self-averaging quantity. This number can be interpreted as the coarse-grained fractal dimension of isolines of H_0.[12–15] On the mathematical side, we are able to show rigorously that the probability $p_{nc}(L)$ that a streamline exceeds a diameter L satisfies the inequality $p_{nc}(L) \leqslant L^{-\alpha}$ for some $\alpha > 0$. Our analysis also shows rigorously that, with probability 1, all streamlines in a given realization are closed, and that the streamline pattern of the flow follows a *hierarchical structure*, with smaller streamlines contained inside larger ones, *ad infinitum*. In particular, the Hamiltonian

$$H_0(x, y) = W_1(y) - W_2(x)$$

has no critical isoline that percolates throughout the plane. This result can be contrasted with the topological analysis of Isichenko *et al.*[12] and Isichenko and Kalda,[13,14] which predicted, generically, a critical percolating level in each realization of a random "monoscale" Hamiltonian. Monoscale Hamiltonians are stationary (i.e., statistically translation-invariant) random functions. Their "statistical topography" was shown to be related to the scaling properties of percolation clusters near the threshold probability.[13,14] Our results suggest that Hamiltonians with long-range correlations satisfying $\langle |H(x, y)|^2 \rangle \approx |x|^q + |y|^q$ for $q > 0$ have a completely different statistical topography. The fact that the streamlines form a hierarchical structure without critical level is of independent interest. It is probably relevant for a first-principles treatment of transport with $\bar{\mathbf{V}} = 0$ in the presence of molecular diffusion.

The second issue is large-scale transport under a nonzero mean velocity. We studied the problem analytically, for $\rho > 1$, and computationally over the entire parameter range. The first point here is the fact that a trapping/percolation transition occurs at $\rho = 1$. For each ρ, we denote by $p_{nc} = p_{nc}(\rho)$ the probability that the streamline starting at the origin remains unbounded or, equivalently, is not a cycle. Numerical simulations show that $0 < p_{nc} < 1$ for $0 < \rho < 1$, and $p_{nc}(\rho) = 1$ for $\rho \geqslant 1$. This fact is also confirmed by rigorous bounds. The trapping/percolation transition has the following implications: In the subcritical regime, the mean position of noncycling particles satisfies

$$\langle \mathbf{r}(t) \rangle_{nc} \simeq \mathbf{r}(0) + \left(\frac{1}{p_{nc}} \bar{\mathbf{V}} \right) t, \qquad t \gg 1$$

where $\langle \cdot \rangle_{nc}$ denotes conditional averaging over realizations for which the particle is free. Thus, at long times, noncycling particles evolve with a larger effective velocity, $(1/p_{nc})\,\bar{\mathbf{V}}$, compensating for the cycling particles which make finite displacements. For this reason, *conditional averaging over noncycling particles* is necessary in order to analyze fluctuations in the subcritical case. In fact, if a front or interface evolves in the "piston-flow" model described previously, a fraction $= 1 - p_{nc}$ of particles is trapped in cycling streamlines and the front moves with an effective velocity $p_{nc}^{-1}\bar{\mathbf{V}}$. The fluctuations of the moving particles are studied by evaluating asymptotically

$$\frac{1}{t^{\nu/2}}\left[\mathbf{r}(t) - \mathbf{r}(0) - \langle \mathbf{r}(t) \rangle_{nc}\right], \qquad t \gg 1$$

the statistics being taken conditionally on noncycling. We find that $= 1$ or $\nu = 3/2$, according to the direction of the mean velocity. Centering the particle position with respect to the *nominal* mean velocity, $\langle \mathbf{r}(t) \rangle = \bar{\mathbf{V}}t$, leads, otherwise, to "ballistic" spreading ($\nu = 2$), due to particles being left behind the front. Of course, in the supercritical case, all particles are free, and averaging is taken with respect to the entire ensemble (Fig. 2). The diagonal-resonant case, $|\bar{V}_1| = |\bar{V}_2| = \bar{U}$, is special because a finite probability exists for particles not to move at all. Studies of particle motion for $\bar{V}_1/\bar{U}$, $\bar{V}_2/\bar{U}$ in a vicinity of this regime reveal a blowup of the effective diffusion coefficient due to a large disparity of particle motions, according to their starting positions. This is a clear example of a phenomenon which cannot be revealed by a mean-field approximation.

As mentioned, the exponent ν depends on the direction of the mean velocity relative to the random grid defining the fluctuations. If $\bar{\mathbf{V}}$ points in the directions $(\pm 1, 0)$, $(0, \pm 1)$ (the *parallel-resonant* case), the motion in the direction transverse to the velocity is Fickian, but the longitudinal fluctuations are superdiffusive, with $\nu = 3/2$. This result applies both in the subcritical and the supercritical regimes. Accordingly, if $\bar{\mathbf{V}} = (\bar{V}_1, 0)$, then $y(t)/\sqrt{t}$ is asymptotically Gaussian with an effective transverse diffusivity $D_{\perp}^{*}$. In the supercritical case, the transverse diffusivity can be computed exactly and is given by

$$D_{\perp}^{*} = \frac{a\bar{U}^2}{2\,|\bar{V}_1|}$$

where a is a microscopic length scale (see Section 2). The (longitudinal) fluctuations in the x coordinate,

$$\frac{1}{t^{3/4}}\left[x(t) - \langle x(t) \rangle_{nc}\right]$$

or

$$\frac{1}{t^{3/4}}\left[x(t)-\bar{V}_1 t\right]$$

(according to whether we consider the subcritical or the supercritical case) converge in distribution to a non-Gaussian random variable. In the supercritical case, we show rigorously that

$$\frac{\langle [x(t)-\bar{V}_1 t]^2\rangle}{t^{3/2}} \sim \frac{a\bar{U}^2}{(2D_\perp^*)^{1/2}}\frac{4}{3}\left(\frac{2}{\pi}\right)^{1/2}$$
$$= a^{1/2}\bar{U}\,|\bar{V}_1|^{1/2}\times 1.06$$

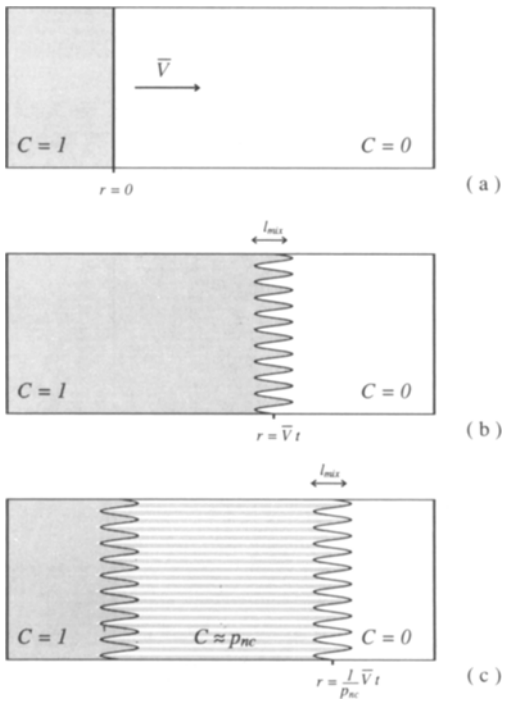

Fig. 2. Schematic representation of the "piston-flow" model. (a) Initial configuration; the gray zone corresponds to the region occupied by the solute. (b) In the supercritical regime all streamlines percolate; the front propagates with a velocity $\bar{\mathbf{V}}$ and develops a mixing zone of width $l_{\max} \propto t^{\nu/2}$ ($\nu = 1$ or 3/2). (c) In the subcritical regime, a fraction $1-p_{nc}$ of particles is trapped in cycling orbits and is progressively left behind the front, while a fraction p_{nc} of free particles moves with an average velocity $p_{nc}^{-1}\bar{\mathbf{V}}$, for $t \gg 1$. The striated region of length $\propto t$, occupied by free particles, has an upwind front with mixing length $\propto t^{\nu/2}$, $\nu = 1$ or 3/2.

The corresponding asymptotic probability density $\bar{P}(x)$ can be characterized as well. Its Fourier transform is given by

$$\hat{\bar{P}}(k) = E\left\{\exp(-(a\bar{U}^2k^2)/[2(2D_\perp^*)^{1/2}] \int_0^1 \int_0^1 \delta(\beta(s)-\beta(s'))\, ds\, ds'\right\} \tag{6}$$

where $\delta(\cdot)$ is the Dirac delta and $E\{\cdot\}$ denotes path integration with respect to a standard Brownian motion $\beta(t)$, $0 \leqslant t \leqslant 1$. The effective transverse diffusivity $D_\perp^*$ appears in the exponential in (6), reflecting the influence of the transverse diffusion on the superdiffusive longitudinal fluctuations. This probability density was obtained previously by Avellaneda and Majda[8,9,16] in the study of a class of models of "nearly stratified" flows with molecular diffusion. It is closely related to the asymptotic probability density for a Brownian walker in a stratified velocity studied by Matheron and de Marsily[7] and later by Zumofen *et al.*[17] The numerical simulations, involving the calculation of various moments, flatness factors, and empirical distributions, strongly suggest that this characterization is qualitatively valid in the subcritical case as well, even for relatively small values of $\rho = |\bar{V}_1|/U$, for which the motion in the x and y directions is strongly coupled. A simple heuristic explanation for this superdiffusion for $\bar{\mathbf{V}} = (\bar{V}_1, 0)$ can be given. In fact, the y component,

$$y(t) = y(0) + \int_0^t U_2(x(s))\, ds$$

experiences random, weakly correlated velocities $U_2(x(s))$ and the Central Limit Theorem applies to the rescaled paths $(1/\sqrt{t})\, y(st)$, $0 < s < 1$, $t \gg 1$. On the other hand, the longitudinal fluctuations satisfy

$$\begin{aligned}\frac{1}{t^{3/4}}\,[x(t) - \langle x(t)\rangle_{nc}] &= t^{-3/4} \int_0^t U_1(y(s))\, ds \\ &= t^{1/4} \int_0^1 U_1\left[t^{1/2}\left(\frac{1}{\sqrt{t}}\, y(st)\right)\right] ds\end{aligned}$$

It can be shown that the stochastic process $t^{1/4}U_1(t^{1/2}y)$ approaches, as $t \to \infty$, a δ-correlated Gaussian white noise and that $(1/\sqrt{t})\, y(st)$ approaches a Brownian motion $(2D_\perp^*)^{1/2}\, \beta(s)$. Moreover, the thermalization time for the transverse motion is much shorter than the corresponding time for the longitudinal motion, which depends on the multiple visits of the walker to the same horizontal layer (see refs. 16 and 17, for example). Therefore, the processes $(1/\sqrt{t})\, y(ts)$, $t^{1/4}U_1(t^{1/2}y)$ "decouple" statistically as $t \gg 1$, and the present model can be mapped into the Matheron–

de Marsily model of a Brownian walker evolving in a random stratified velocity.

If the velocity $\bar{\mathbf{V}}$ is not perfectly aligned with the coordinate directions, i.e., $\bar{V}_1 \bar{V}_2 \neq 0$, the motion is Fickian for both the x and y directions, in the subcritical and supercritical regimes. Remarkably, if either $|\bar{V}_1|$ or $|\bar{V}_2|$ exceeds the amplitude of the fluctuations $|\bar{U}|$, i.e., $\rho > 1$, the corresponding diffusivities can be computed analytically. We find that

$$D_{11}^* = \frac{a\bar{U}^2}{2|\bar{V}_2|}\left(1 + \frac{|\bar{V}_1|\,\bar{U}^2}{|\bar{V}_1| \cdot |\bar{V}_2^2 - \bar{U}^2| + |\bar{V}_2| \cdot |\bar{V}_1^2 - \bar{U}^2|}\right) \tag{7a}$$

and

$$D_{22}^* = \frac{a\bar{U}^2}{2|\bar{V}_1|}\left(1 + \frac{|\bar{V}_2|\,\bar{U}^2}{|\bar{V}_1| \cdot |\bar{V}_2^2 - \bar{U}^2| + |\bar{V}_2| \cdot |\bar{V}_1^2 - U^2|}\right) \tag{7b}$$

Notice that D_{11}^* and D_{22}^* diverge as $\bar{V}_1$ and $\bar{V}_2$ approach the diagonal-resonant values $|\bar{V}_1| = |\bar{V}_2| = \bar{U}$, reflecting the enhancement of the dispersion caused by the trapping of a fraction of the particles in "pockets" in which the mean velocity cancels the fluctuations almost completely. The Monte Carlo simulations allow us to investigate particle dispersion in all regimes and, in particular, in the subcritical regime for which analytical formulas for the diffusivities are not available near resonance or near $\rho = 0$. The calculations confirm Fick's law for $\bar{V}_1 \bar{V}_2 \neq 0$ and provide numerical values for the diffusivities. We focused, in particular, on the values of the dimensionless ratios

$$r_{ii} = D_{ii}^*/(a\bar{U}^2/2\bar{V}_j), \qquad i \neq j, \quad i, j = 0 \text{ or } 1$$

Here, $a\bar{U}^2/2\bar{V}_j$ represents the diffusivity from the standard Kubo weak-coupling approximation,[18,19] which is exact in the limit $\rho \gg 1$. The numerical simulations show that r_{ij} increases as $\rho \to 0$, in the subcritical regime, and blows up near the diagonal resonance $|\bar{V}| = |\bar{V}_2| \sim \bar{U}$.

In the final portion of the paper we compare the values of r_{ii} with the predictions of the direct interaction approximation, which is a mean-field approximation for D_{ii}^* based on the input of the two-point correlation function of the velocity, and the mean velocities $\bar{V}_1$ and $\bar{V}_2$. It is shown that this approximation does not account for the observed increase in r_{ii} for $\rho \ll 1$ or near the resonances. The exact values of the diffusivities are compared with the DIA for a variety of values of $\bar{V}_1$ and $\bar{V}_2$ as well. Good agreement between DIA and the exact formulas is found only for certain nonresonant values of $\bar{\mathbf{V}}$ such that $\bar{V}_1 \cong \bar{V}_2$, or for $\rho \gg 1$.

The contents of the paper are as follows: in Section 2 we give a detailed description of the statistical model. In Section 3 we discuss the statistical topography of streamlines, and the estimates for the distribution of the streamline diameters and of their fractal dimension. In Section 4 we study the supercritical regime, deriving exact results for the long-time particle dynamics analytically. Section 5 discusses the Monte Carlo simulations, which are carried out in both the critical and subcritical regimes, including the parallel-resonant and diagonal-resonant cases. In Section 6 the numerical aspects of the simulation, and, in particular, its efficiency on the CM parallel machine are discussed. The general conclusions are drawn in Section 7, after detailed comparisons with the Isichenko–Kalda theory and the DIA are made.

2. DESCRIPTION OF THE MODEL

The velocity field $\mathbf{U} = (U_1, U_2)$ is constructed by means of an auxiliary random grid. Specifically, consider two independent Poisson processes with unit intensity,

$$\cdots X_{-k}, X_{-k+1}, \ldots, X_0, X_1, \ldots, X_k, \ldots$$

and

$$\cdots Y_{-l}, Y_{-l+1}, Y_{l+2}, \ldots, Y_0, Y_1, \ldots, Y_l, \ldots$$

The indices in both sequences vary from $-\infty$ to $+\infty$ over the integers, i.e., the sequences are doubly infinite. According to basic properties of the Poisson statistics, the differences $X_k - X_{k-1}$, $Y_l - Y_{l-1}$, $k, l = 0, \pm 1, \pm 2, \ldots$, are independent random variables with exponential distributions, so that

$$\text{Prob}\{X_k - X_{k-1} > \alpha\} = \text{Prob}\{Y_l - Y_{l-1} > \alpha\} = e^{-\alpha}, \quad \alpha > 0$$

We consider the random grid in the x–y plane formed by the parallel vertical lines

$$x = aX_k, \qquad k \text{ integer}$$

and the parallel horizontal lines

$$y = aY_l, \qquad l \text{ integer}$$

where a is a constant with dimensions of length. The spacings between consecutive parallel lines are exponentially distributed with mean a. This grid subdivides the plane into rectangular cells

$$\begin{aligned} aX_k < x < aX_{k+1} \\ aY_l < y < aY_{l+1} \end{aligned} \tag{8}$$

The fluctuating stochastic velocity field $\mathbf{U}(x, y)$ is defined to be constant in each cell. In the cell (8) corresponding to the integers (k, l) we define

$$U_1 = (-1)^l \bar{U}, \qquad U_2 = (-1)^k \bar{U} \tag{9}$$

where $\bar{U}$ is a positive constant with dimensions of velocity. Consequently, we have $\mathbf{U} = (\pm \bar{U}, \pm \bar{U})$, with signs varying according to the cell location. From this definition, the horizontal component U_1 depends only on the "row" on which it is defined, through the integer l, and the vertical component depends only on its "column," so that

$$U_1 = U_1(y), \qquad U_2 = U_2(x) \tag{10}$$

In particular, $\mathbf{U}(x, y) = (U_1(y), U_2(x)) = (U_1(y), 0) + (0, U_2(x))$ is a superposition of two stratified random velocities perpendicular to one another. Because of this, the normal components of $\mathbf{U}$ are continuous across cell boundaries (Fig. 3). The motion of a particle under $\mathbf{U}$,

$$\begin{aligned} \frac{dx(t)}{dt} &= U_1(y(t)) \\ \frac{dy(t)}{dt} &= U_2(x(t)) \end{aligned} \tag{11}$$

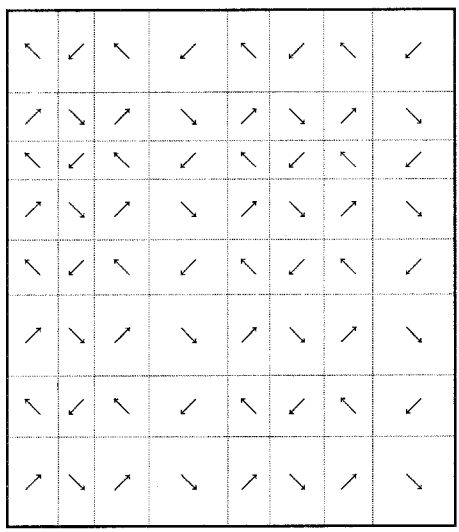

Fig. 3. A realization of the random velocity field $\mathbf{U}(x, y)$ (schematic). The velocities point in four possible directions $(\pm 1, \pm 1)$; note that the normal components across cell boundaries are continuous.

is defined as follows: a particle located initially inside a cell is advected with the uniform velocity $(\pm \bar{U}, \pm \bar{U})$ until it hits a cell boundary. At the cell boundary the path is "bent" by an angle of 90° according to the sign change in the tangential component. The motion for particles originating at a cell boundary is well defined (the particle moves *into* a cell according to the value of the normal velocity), except if the particle originates at a *cell corner*, where the velocity is not clearly defined. We remove this ambiguity by defining the velocity to be zero at cell corners, so that, if a particle reaches a corner it remains there and if it originates at a corner it does not move. Notice that the cell corners, which have coordinates (aX_k, aY_l), $k, l = 0, \pm 1, \pm 2, \ldots$, are countable and hence the probability that a given point in the plane coincides with any such stagnation point is zero. Examination of the flow near these stagnation points shows that they are either "O-points" or "X-points" in the terminology of Soward and Childress,[20] the former being circulation points and the latter unstable fixed points with two incoming and two outgoing trajectories. The X-points and the O-points are alternating in each horizontal and vertical line; if k and l have the same parity, (aX_k, aY_l) is an X-point, and if k and l have different parity, (aX_k, aY_l) is an O-point. Clearly, the set of trajectories passing through either an O or an X point is countable, and hence statistically negligible. The flow (11) admits a Hamiltonian, i.e., can be written in the form $dx/dt = \partial H_0/\partial y$, $dy/dt = -\partial H_0/\partial x$, with

$$\begin{aligned} H_0(x, y) &= \int_0^y U_1(y')\, dy' - \int_0^x U_2(x')\, dx' \\ &\equiv W_1(y) - W_2(x) \end{aligned} \tag{12}$$

Notice that the functions W_i are piecewise linear, having slopes $\pm \bar{U}$, which are constant over intervals that are exponentially distributed with mean a. Thus, $W_1(y)$ and $W_2(x)$ are standard, continuous-time random walks.

The statistical properties of Poisson processes imply that $U_1(y)$ and $U_2(x)$ are two-state Markov processes, and that the random field $\mathbf{U}(x, y) = (U_1(y), U_2(x))$ is statistically translation invariant and ergodic. One can easily compute the first and second moments of U_i, which are given by

$$\begin{aligned} \langle U_1(y) \rangle &= \langle U_2(x) \rangle = 0 \\ \langle U_1(y)\, U_1(y') \rangle &= \bar{U}^2 e^{-2|y-y'|/a} \\ \langle U_2(x)\, U_2(x') \rangle &= \bar{U}^2 e^{-2|x-x'|/a} \end{aligned} \tag{13}$$

Despite the short-range correlations of U_1 and U_2, points which have approximately the same x or y coordinate have strongly correlated

velocities even if they are far apart, because of the special structure (10). Notice also that this random field has cubic symmetry: the Hamiltonian is statistically invariant under reflections about axes parallel to (1, 0), (0, 1), (1, 1), and (1, −1). Higher degrees of symmetry can be achieved by considering Hamiltonians such as (5).

To better understand the "universality class" to which this model belongs, we note that, from (12), (13),

$$\langle |H_0(x, y)|^2 \rangle \propto a\bar{U}^2 |y|, \qquad |y| \gg 1$$
$$\propto a\bar{U}^2 |x|, \qquad |x| \gg 1$$

Therefore, if we consider a coarse-grained limit of $H_0(x, y)$ as $a \to 0$, $\bar{U} \to +\infty$ with $aU^2 = 1$, we obtain, by a simple application of the Central Limit Theorem,

$$H_0(x, y) \approx B_1(y) - B_2(x)$$

where $B_1(y)$, $B_2(x)$ are independent, standard Brownian motions. Hence, the corresponding "coarse-grained" velocity is formally

$$[N_1(y), N_2(x)] \tag{14}$$

where $N_i = B_i'$ are independent, Gaussian white-noise processes. [Note, however, that in this limit, the equations of motion (11) are not well defined, because N_i, $i = 1, 2$, are not differentiable.] We believe that the results presented in Section 3 for the velocity **U** also apply to the more general class of flows which are "smoothed-out" versions of the white-noise velocity (14).

In the case of motion under a nonzero mean velocity, we take

$$\mathbf{V}(x, y) = (\bar{V}_1 + U_1(y), \bar{V}_2 + U_2(x))$$

where $\bar{V}_1$ and $\bar{V}_2$ are constants with dimensions of velocity. The random field **V** is again constant in each rectangular cell of the grid, and takes the values $(\bar{V}_1 \pm \bar{U}, \bar{V}_2 \pm \bar{U})$ according to (9). The addition of a constant velocity preserves continuity of the normal components across cell boundaries, and thus the flow is well defined except at the cell corners, where it is defined to be zero. Clearly, the corresponding flow, described by (3), is Hamiltonian, with

$$H(x, y) = \bar{V}_1 y - \bar{V}_2 x + H_0(x, y)$$

A fundamental difference between the cases $\bar{V} = 0$ and $\bar{V} \neq 0$ is that in the former case the streamlines of $\mathbf{V}(x, y)$ are closed and bounded with

probability 1, while for $\bar{V} \neq 0$ a fraction of streamlines is unbounded. The fraction of unbounded streamlines depends on ρ, the mean-to-fluctuations ratio (Section 3).

The diagonal-resonant case $|\bar{V}_1| \cong |\bar{V}_2| \cong \bar{U}$ is special. Near these parameter values some cells can have almost zero velocity, since $\mathbf{V} = (\bar{V}_1 \pm \bar{U}, \bar{V}_2 \pm \bar{U})$. This corresponds to the physical situation in which the amplitudes of the mean flow and the fluctuations are nearly equal and both fields cancel each other out in certain regions of the medium, producing "pockets" of stagnation. For values of $\bar{V}_1$, $\bar{V}_2$ near this resonance, a randomly chosen realization will result in very small particle displacement for 25% of the initial positions (one cell out of four) and much larger displacements in the remaining 75%.

3. STATISTICAL TOPOGRAPHY OF THE HAMILTONIANS H_0 AND H

3.1. $\bar{V} = 0$

We examine more closely the structure of the streamlines solving the flow equations (3), focusing first on the "zero-mean-velocity" case, $\bar{\mathbf{V}} = 0$, and subsequently on the case $\bar{\mathbf{V}} \neq 0$. We shall see that the presence of a nonzero mean velocity alters substantially the topology of the flow and consequently its long-time behavior. It is useful to define the notion of *percolation of streamlines* for a random flow. A streamline, or solution of (3) for $-\infty < t < +\infty$, is said to *percolate* if it is spatially unbounded so that a particle originating at time $t = 0$ on it will be eventually at arbitrarily large distances from its initial position. In particular, such streamlines have the property that, given a "box" of side L centered at the starting point, the streamline exits the box after some time t, and this happens for all box sizes L. This motivates our use of the term percolation. If a streamline does not percolate, then either (i) it terminates at an unstable fixed point located at a cell corner or (ii) it forms a closed trajectory along which it undergoes periodic motion. The first case is negligible from a statistical viewpoint because the set of streamlines terminating at an unstable fixed point is countable. The overall "statistical topography" of the flow with $\bar{\mathbf{V}} = 0$ is characterized precisely in the following results.

Theorem 1. If $\bar{\mathbf{V}} = 0$, then, with probability one over the set of velocity realizations, (a) there exist *no* percolating streamlines, and (b) all streamlines terminating at an unstable fixed point (X-point) originate also from the same fixed point, forming a closed "loop."

Proof. The proof of (a) hinges on the following proposition:

Proposition 2. Let E_L denote the event

$$E_L = \{\text{for all points } (x, y) \text{ lying on the boundary of the square of side } 2L \text{ centered at } (0, 0), \text{ we have } H_0(x, y) < -2\,|\bar{U}|\}$$

Then

$$\text{Prob}\left\{\bigcup_{N=1}^{\infty} E_N\right\} = 1$$

In words, the assertion is that there exists a set of unit probability in the space of velocity configurations, such that the Hamiltonian $H_0(x, y) = W_1(y) - W_2(x)$ will be uniformly negative, less than -2, on the boundary of *some* square box centered at $(0, 0)$. The box may depend on the particular configuration. The proof of this proposition is sketched in Appendix A; for a general proof which applies to an arbitrary Hamiltonian of the form (5) see Apelian.[21] Assuming that Proposition 2 is true, consider a disk of radius 1 centered about $(0, 0)$. Then, since $|\partial H/\partial x| = |\partial H/\partial y| = |\bar{U}|$, we have

$$|H(x, y)| \leqslant (|x| + |y|)\,|\bar{U}| \leqslant |\bar{U}|\sqrt{2} < 2\,|\bar{U}|$$

for (x, y) inside the disk. According to Proposition 2, the Hamiltonian satisfies $H(\tilde{x}, \tilde{y}) < -2\,|\bar{U}|$ for all points $(\tilde{x}, \tilde{y})$ on the boundary of some square box centered about $(0, 0)$ of side $\geqslant 2$, containing the unit disk about $(0, 0)$. Therefore, no isoline of H passing through the disk can cross the boundary of the square—otherwise $|H(\tilde{x}, \tilde{y})| < 2\,|\bar{U}|$ on the boundary of the square at some point. We conclude that *all streamlines originating from the unit disk around* $(0, 0)$ *are bounded, with probability one.*

To conclude that there exist no unbounded streamlines for velocities in a set of configurations of measure 1, we argue as follows: let $D_1, D_2, D_3, \ldots$ denote a countable collection of disks of unit radius covering the x–y plane. Then, if an infinite streamline exists, it must pass through infinitely many and hence at least one D_j, $j = 0, 1, 2, \ldots$. Therefore

$$\begin{aligned}\text{Prob}\{\text{infinite streamline}\} &= \text{Prob}\{\text{infinite streamline and it passes through } D \text{ for some } j\} \\ &\leqslant \sum_{j=1}^{\infty} \text{Prob}\{\text{infinite streamline that passes through } D_j\} \qquad (15)\end{aligned}$$

Because the statistics are translation invariant, we have

$$\begin{aligned}&\text{Prob}\{\text{infinite streamline that passes through } D_j\}\\&\quad=\text{Prob}\{\text{infinite streamline that passes through}\\&\qquad\text{the unit disk centered at } (0,0)\}\\&\quad=0\end{aligned}$$

Hence, all the summands in (15) vanish and *the probability that a configurations has an infinite streamline is zero.*

To prove (b), we show that a streamline connecting two *different* unstable fixed points occurs with zero probability. For this, let us calculate the probability that, for given k, l, m, n, the points (aX_k, aY_l), (aX_m, aY_n) are connected by a streamline. If they are connected, then they must lie at the same level, i.e., $H_0(aX_k, aX_l) = H_0(aX_m, aY_n)$. However,

$$\begin{aligned}H_0(aX_k, aY_l) - H_0(aX_m, aY_n) = [W_1(aY_n) - W_1(aY_l)]\\ - [W_2(aX_m) - W_2(aX_k)]\end{aligned} \tag{16}$$

The terms in brackets are sums of independent, exponentially distributed random variables. For instance, we have

$$\begin{aligned}W_1(aY_n) - W_1(aY_l) &= \int_{aY_l}^{aY_n} U_1(y)\,dy\\ &= \sum_{j=l+1}^{n} (-1)^j \bar{U}a(Y_j - Y_{j-1})\end{aligned}$$

and similarly for the second summand. Hence (16) reduces to

$$\sum_{j=l+1}^{n} (-1)^j (Y_j - Y_{j-1}) = \sum_{i=k+1}^{m} (-1)^i (X_i - X_{i-1})$$

Since the differences are independent and exponentially distributed, the probability that this equation is satisfied is ze. This shows that the probability that two given different X-points are connected by a streamline is 0. Finally, since the set of all unstable points is countable, the probability that *any* pair of unstable points is linked by a streamline is also 0, concluding the proof of Theorem 1. ■

From Theorem 1, we conclude that the structure of the streamlines of the flow with $\bar{\mathbf{V}} = 0$ is as follows: all streamlines are closed and correspond to cycling motion of particles, with the exception of homoclinic closed loops which begin and end at the same unstable fixed point. Each unstable fixed point is associated with two loops, and, topologically, two types of

configurations are possible at each of the fixed points. The first case corresponds to a pair of loops which have nonoverlapping interiors (a "figure 8" configuration) and the second to a pair of loops such that the interior of one is contained in the other ("self-enclosing" streamline); these two loops are represented in Figs. 4a and 4b. (See also Isichenko.[15]) The global picture that arises is that of a flow with a hierarchy of larger and larger closed loops passing through unstable X-points and containing closed streamlines (see Fig. 4c).

Theorem 1 can be contrasted with the topological analysis of Isichenko *et al.*[12] and Isichenko and Kalda,[13,14] in which a critical infinite streamline was postulated to exist in *every* realization of a generic random Hamiltonian. The reason for the discrepancy is that those authors studied "monoscale" random functions which are stationary processes and, in particular, have bounded rms amplitudes as $(x, y) \to +\infty$. We believe

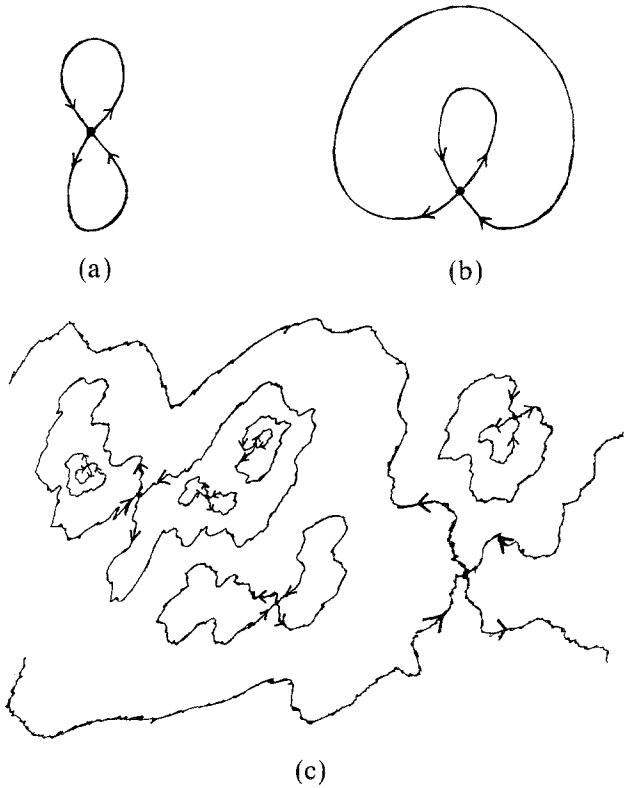

Fig. 4. (a) A "figure 8" configuration: two homoclinic loops with the same orientation linked at an X-point; (b) "self-enclosed" streamline: two loops with opposite orientation linked at an X-point; (c) schematic rendering of the streamline hierarchical structure.

that the present hierarchical topology of closed streamlines without critical level is characteristic of random Hamiltonians with unbounded growth. We shall return to this point later (Section 7.1).

The distribution of sizes of streamlines and their lengths can be analyzed by Monte Carlo simulations, using large "boxes" in which configurations are simulated and subsequently measuring the probability that a streamline exists the box, the length of such streamlines, etc. For this we define

$$p_{nc}(L) = \text{Prob}\{|\mathbf{r}(t)| > L \text{ for some } t, \text{ given that } \mathbf{r}(0) = 0\}$$

Our simulations consisted in generating 8192 independent configurations of sizes up to $L = a2^{15}$ and measuring the probability of exit. We found that p_{nc} satisfies the power law

$$p_{nc}(L) \propto L^{\alpha}, \qquad L \gg 1, \qquad \alpha = 0.21 \pm 0.017 \tag{17}$$

(See Fig. 5.) We can also prove a rigorous result which gives a qualitative upper bound for $p_{nc}(L)$, which we state as follows.

Proposition 3. There exists a positive number α such that

$$p_{nc}(L) \leqslant L^{-\alpha}$$

For a sketch of the proof see Appendix A. A more complete analysis is given in Apelian.[21]

A characteristic property of very long streamlines of random Hamiltonians, first observed and studied by Isichenko and co-workers,[12–14]

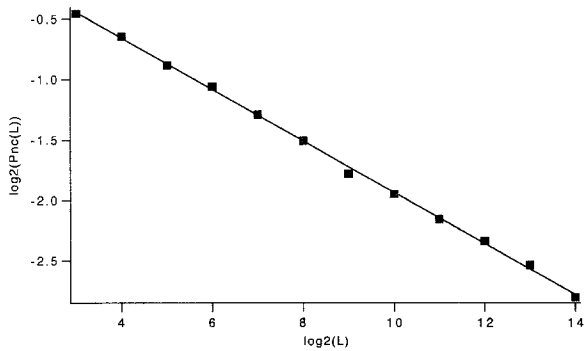

Fig. 5. Log–log plot showing the dependence of the escape probability $p_{nc}(L)$ on the box size L. This simulation uses 8192 random realizations of $\mathbf{V}$, tracking the position of a particle originating at (0, 0) for each realization.

is fractal behavior on a coarse-grained scale. This means that streamlines with diameter $>L$ should have a length $\lambda(L)$ (measured in units of the ultraviolet length a) which scales superlinearly, i.e., $\lambda(L)/a \sim (L/a)^{\gamma}$, $\gamma > 1$. The exponent γ represents the fractal dimension of the streamlines.[12–15] To calculate γ for our model, we measured the length of the streamlines exiting a hierarchy of boxes of size $L \simeq 2^k$, $k \leqslant 15$, and averaged over the number of exiting particles. The computational result is

$$\frac{\langle \lambda(L) \rangle}{a} \propto \left(\frac{L}{a}\right)^{\gamma}, \qquad L \gg 1, \quad \gamma = 1.28 \pm 0.015$$

In Fig. 6 we give a log–log plot of $\langle \lambda(L) \rangle / a$ versus L/a. Error bars on the exponents α and γ can be determined in the following way. Since we simulated 8192 independent environments, the error on $p_{nc}(L)$ for each L is of order $(4 \times 8192)^{-1/2} = 0.006$, the factor of 4 arising from the fact that the variance of Bernoulli trials with unknown probability is $\leqslant 1/4$. We then did a straight-line fit of the points $(\log L, \log\langle p_{nc}(L) \rangle)$, where $\log\langle p_{nc}(L) \rangle$ is the logarithm of the frequency of exiting particles. A slope of $\alpha \simeq 0.21$ was observed, with rms distance for the last 12 points $\sigma_{\alpha} = 0.017$. The agreement with the linear fit is remarkable. We conclude that the error on α is ± 0.017.

We turn next to the analysis of the estimate of the fractal dimension of the long streamlines, i.e., the exponent γ. Actually, it is possible to obtain γ in two independent ways. First, we can use the exact sum rule

$$\alpha + \gamma = 2 - h = 1.5$$

where $h = 1/2$ is the Hölder exponent of H_0.[13] This gives the estimate $\gamma = 1.5 - 0.21 \pm 0.017 = 1.29 \pm 0.017$. Alternatively, as mentioned above, we

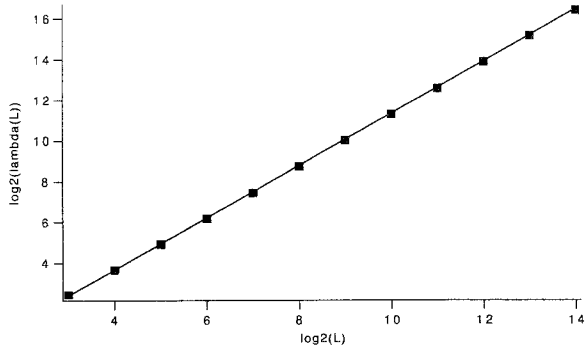

Fig. 6. Log–log plot showing the behavior of $\langle \lambda(L) \rangle$, the mean length of the streamlines percolating outside a box of size L.

can compute γ by a linear regression on the data ($\log L$, $\log\langle\lambda(L)\rangle$), where the average is taken over trajectories which exit the box of size L. This regression gives the estimate $\gamma \simeq 1.28$ with rms distance for the last 12 points $\sigma_\gamma = 0.015$. Using the two independently computed exponents, we obtain $\alpha + \gamma = 1.49 \pm 0.03$, which is in excellent agreement with the sum rule. Thus, we can safely conclude that the error bar for γ is $\leqslant 0.02$.

It is interesting to note that the scatter from the least-squares linear fit is quite negligible, despite the fact that fewer and fewer particles exit the longer boxes and contribute to the average $\langle\lambda(L)\rangle$. A plausible explanation for this phenomenon is that the fractal exponent γ is a self-averaging quantity which should not vary from one realization to another. This explanation can be made into a rigorous mathematical theorem by an appropriate definition of $\lambda(L)$ and the study of the properties of thermodynamic limit[21]

$$\lim_{L\to\infty} \frac{\log \lambda(L)}{\log L}$$

3.2. $\bar{V} \neq 0$

The presence of a mean velocity changes the streamline picture substantially, giving rise to the elongation of closed streamlines in the direction of $\bar{V}$ and the "opening" of a fraction of streamlines. The relevant parameter to measure the relative effects of mean velocity/fluctuations is

$$\rho = \frac{\max(|\bar{V}_1|, |\bar{V}_2|)}{|\bar{U}|}$$

In the supercritical case ($\rho \geqslant 1$) all streamlines are open. In fact, if, for instance, $\bar{V}_1 > |\bar{U}|$, then

$$\begin{aligned} \frac{dx(t)}{dt} &= \bar{V}_1 + U_1(y(t)) \\ &\geqslant \bar{V}_1 - |\bar{U}| \\ &\geqslant 0 \end{aligned} \tag{18}$$

and hence particles always move in the upwind direction. Let $p_{nc} = p_{nc}(\rho)$ denote the probability of not cycling, or percolating, starting from $\mathbf{r}(0) = (0, 0)$. (This notation emphasizes the dependence of p_{nc} on ρ, the "box size" now being infinite.) In the subcritical regime ($0 < \rho < 1$), $p_{nc}(\rho)$ satisfies $0 < p_{nc}(\rho) < 1$. This is demonstrated rigorously in Proposition 4 below. Equating ensemble averages with spatial averages over a given

realization, by means of the ergodic theorem, we conclude that, *with probability* 1, *in the subcritical regime a given realization will contain a fraction* $1-p_{nc}(\rho)$ *of closed streamlines and a fraction* $p_{nc}(\rho)$ *of open streamlines.*

Proposition 4. Assume that $0<\rho<1$. Then

$$\frac{\rho}{1+\rho} \leqslant p_{nc}(\rho) < 1 \tag{19}$$

Proof of Proposition 4. To establish the lower estimate in (19), assume without loss of generality that $\bar{V}_1 > 0$, $|V_2| < |V_1| < |\bar{U}|$ and introduce the set E_δ of realizations such that the trajectory originating at $\mathbf{r}(0) = (0, 0)$ satisfies

$$|\mathbf{r}(t)| \leqslant \delta, \qquad \text{for all } t$$

Then

$$\begin{aligned} \bar{V}_1 t &= \langle x(t) \rangle \\ &= \langle x(t) \mid E_\delta \rangle P(E_\delta) + \langle x(t) \mid E_\delta^c \rangle P(E_\delta^c) \end{aligned} \tag{20}$$

where $\langle \cdot \mid A \rangle$ denotes conditional expectation with respect to A, and E_δ^c is the complement of E_δ. The x coordinate satisfies the absolute bound

$$x(t) \leqslant (\bar{V}_1 + |\bar{U}|)\, t$$

Substituting in (20), we obtain

$$\bar{V}_1 t \leqslant \langle x(t) \mid E_\delta \rangle P(E_\delta) + (\bar{V}_1 + |\bar{U}|)\, t P(E_\delta^c)$$

Dividing both sides of this inequality by $(\bar{V}_1 + |\bar{U}|)\, t$, we obtain

$$\frac{\bar{V}_1}{\bar{V}_1 + |\bar{U}|} \leqslant \frac{\langle x(t) \mid E_\delta \rangle P(E_\delta)}{(\bar{V}_1 + |\bar{U}|)\, t} + P(E_\delta^c)$$

The conditional average $\langle x(t) \mid E_\delta \rangle$ is bounded from above by δ, from the definition of the set E_δ. Therefore, letting $t \to \infty$, we obtain

$$\frac{\bar{V}_1}{\bar{V}_1 + |\bar{U}|} \leqslant P(E_\delta^c) \tag{21}$$

for any value of δ. Notice that $\bigcap_{N=1}^{\infty} E_N^c = \{\text{set of environments for which } (\mathbf{r}(t),\, t \geqslant 0) \text{ percolates}\}$. Hence, letting $\delta \to \infty$ in (21), we conclude that

$$p_{nc} \geqslant \frac{\bar{V}_1}{\bar{V}_1 + |\bar{U}|} = \frac{\rho}{1+\rho}$$

which is the lower bound in (19).

The upper estimate in (19) is obtained as follows. If $\rho < 1$, then the horizontal velocity components are $\bar{V}_1 + \bar{U}$ and $\bar{V}_1 - \bar{U}$ and these two numbers have opposite signs. Analogously, the vertical components $\bar{V}_2 + \bar{U}$ and $\bar{V}_2 - \bar{U}$ have different signs. In particular, a particle can travel "downwind" as well as "upwind" and form a closed path. The simplest possible closed configuration that can arise is a polygonal curve with four sides winding about an O-point. Let (aX_k, aY_l) be the O-point which is nearest to $(0, 0) = \mathbf{r}(0)$. It is easy to see that the streamline passing through $(0, 0)$ will wind around (aX_k, aY_l) and form a four-sided polygon provided that the four X-points which are nearest to the O-point are sufficiently far from it. The probability of configurations of nearest neighbors (in terms of the Poisson processes $\{X_k\}$, $\{Y_l\}$) leading to a closed, four-sided loop can be estimated, using the fact that the nearest-neighbor distances to the grid are exponentially distributed and independent. A tedious but straightforward computation shows that the probability p_{loop} that the origin lies in a simple four-sided loop is positive for $\rho < 1$. Therefore, $p_{nc} < 1 - p_{\text{loop}} < 1$. ■

We have computed a few values of $p_{nc}(\rho)$ for $\bar{\mathbf{V}} = (\bar{V}_1, 0)$, which are shown in Table I.

Finally, we calculate the effective mean velocity of noncyclying particles in the subcritical regime. Introduce the set E of realizations such that the streamline originating at $\mathbf{r}(0) = (0, 0)$ percolates. Then,

$$\begin{aligned} \bar{\mathbf{V}}t &= \langle \mathbf{r}(t) \rangle \\ &= \langle \mathbf{r}(t) \mid E \rangle\, p_{nc} + \langle \mathbf{r}(t) \mid E^c \rangle (1 - p_{nc}) \end{aligned} \tag{22}$$

Clearly, on the configurations of E^c, $\mathbf{r}(t)$ is a cycling path which satisfies

Table I. Probability That the Streamline Passing through (0, 0) Is Open, for Different Values of $\rho = \bar{V}_1/\bar{U}$[a]

$\rho(= \bar{V}_1/\bar{U})$	$p_{nc}(\rho)$
0.125	0.391113
0.250	0.526367
0.375	0.620605
0.500	0.707031
0.625	0.765137
0.750	0.835449
0.875	0.900391

[a] The mean velocity satisfies $\bar{V}_2 = 0$.

$\lim_{t\to\infty}(1/t)\,|\mathbf{r}(t)|=0$. Since the ratio $(1/t)\,|\mathbf{r}(t)|$ is uniformly bounded, by the Dominated Convergence Theorem,

$$\lim_{t\to\infty}\frac{1}{t}\langle\mathbf{r}(t)\mid E^c\rangle=0$$

Therefore, dividing (22) by t, and letting $t\to\infty$, we obtain

$$\lim_{t\to\infty}\frac{1}{t}\langle\mathbf{r}(t)\rangle_{nc}\equiv\lim_{t\to\infty}\frac{1}{t}\langle\mathbf{r}(t)\mid E\rangle$$

$$=\frac{1}{p_{nc}}\bar{\mathbf{V}}$$

This means that if $0<\rho<1$, *the fraction of "free" particles moves, for* $t\gg 1$, *with an effective velocity* $(1/p_{nc})\,\bar{\mathbf{V}}$. This velocity is larger than the nominal velocity $\bar{\mathbf{V}}$, and compensates for the fraction of trapped particles so as to have $\bar{\mathbf{V}}t=\langle\mathbf{r}(t)\rangle$, which is a consequence of the incompressibility of $\mathbf{V}$.

4. RIGOROUS ANALYSIS OF THE SUPERCRITICAL CASE

4.1. Mean Square Displacements

Remarkably, if $\rho\geqslant 1$, the model is completely solvable and we can calculate explicitly the mean-square displacement, $\langle|\mathbf{r}(t)-\bar{\mathbf{V}}t|^2\rangle$ as $t\to\infty$. This can be done for all velocities such that $\max(|\bar{V}_1/\bar{U}|,\,|\bar{V}_2|/\bar{U})\geqslant 1$, including velocities in a vicinity of the diagonal-resonant case $|\bar{V}_1|\sim\bar{U}$, $|\bar{V}_2|\sim\bar{U}$ and in the parallel-resonant case ($\bar{V}_1\bar{V}_2=0$), for which the longitudinal fluctuations are superdiffusive. The exact solvability of the model for $\rho\geqslant 1$ is due to the fact that, in this regime, one or both coordinates are *monotone functions of time* [cf. Eq. (18)]. Expressing time as a function of the increasing coordinate and substituting in the other one, we obtain a Markov process which can be analyzed precisely. In the new coordinates, mean-square displacements can be computed through somewhat involved manipulations.

We summarize the results of the calculations for the mean-square displacements in the following result.

Theorem 5. (i) If $\bar{V}_1\cdot\bar{V}_2\neq 0$ and $\rho>1$, then

$$D_{11}^{*}\equiv\lim_{t\to\infty}\frac{1}{2t}\langle[x(t)-\bar{V}_1 t]^2\rangle$$

$$=\frac{a\bar{U}^2}{2\,|\bar{V}_2|}\left(1+\frac{|\bar{V}_1|\,\bar{U}^2}{|\bar{V}_2|\cdot|\bar{V}_1^2-\bar{U}^2|+|\bar{V}_1|\cdot|\bar{V}_2^2-\bar{U}^2|}\right)\tag{23}$$

and, similarly,

$$D_{22}^* \equiv \lim_{t\to\infty} \frac{1}{2t} \langle [y(t) - \bar{V}_2 t]^2 \rangle$$

$$= \frac{a\bar{U}^2}{2|\bar{V}_1|} \left(1 + \frac{|\bar{V}_2|\,\bar{U}^2}{|\bar{V}_2| \cdot |\bar{V}_1^2 - \bar{U}^2| + |\bar{V}_1| \cdot |\bar{V}_2^2 - \bar{U}^2|} \right) \tag{24}$$

(ii) If $\bar{V}_1 \cdot \bar{V}_2 = 0$ and $\rho > 1$, the transverse motion is diffusive and the longitudinal motion is superdiffusive. Accordingly, if $|\bar{V}_1| > |\bar{U}|$ and $\bar{V}_2 = 0$, then

$$D_{22}^* = D_\perp^* = \lim_{t\to\infty} \frac{1}{2t} \langle [y(t)]^2 \rangle = \frac{a\bar{U}^2}{2|\bar{V}_1|} \tag{24'}$$

and

$$\lim_{t\to\infty} \frac{\langle [x(t) - \bar{V}_1 t]^2 \rangle}{t^{3/2}} = \left[\frac{4}{3} \left(\frac{2}{\pi} \right)^{1/2} \right] \frac{a\bar{U}^2}{(2D_\perp^*)^{1/2}}$$

$$= \left[\frac{4}{3} \left(\frac{2}{\pi} \right)^{1/2} \right] a^{1/2} \bar{U} |V_1|^{1/2} \tag{25}$$

Proof. Assume, without loss of generality, that $\bar{V}_1 > \bar{U}$ and that $\bar{V}_2 \geqslant 0$. For simplicity in the computations, it is convenient to use the dimensionless space, time, and velocity scales defined by

$$\begin{aligned} x' &= x/a \\ y' &= y/a \\ t' &= t\bar{U}/a \\ \mathbf{V}' &= (1/\bar{U})\,\mathbf{V} \end{aligned} \tag{26}$$

In the new variables the "microscopic" length scale (grid separation) and time scale are unity and the velocity fluctuations are ± 1. The only remaining parameters are $\bar{V}_1/\bar{U}$ and $\bar{V}_2/\bar{U}$, the dimensionless mean velocities. We shall compute the mean-square displacements in dimensionless variables and obtain the dimensional results by restoring units. Accordingly, we shall assume that $a = 1$ and $\bar{U} = 1$ in the basic equations (3); this is equivalent to the proposed nondimensionalization. Note that the supercritical regime corresponds now to $\max(|\bar{V}_1|, |\bar{V}_2|) \geqslant 1$, and our assumption becomes $\bar{V}_1 > 1$, $\bar{V}_2 \geqslant 0$.

First we describe the "Markovianization" arising from $\bar{V}_1 > 1$. Because

of this assumption, $x(t)$ is an increasing function of t. Therefore, we can parametrize the coordinate y and the time t as functions of x:

$$y = y(x)$$
$$t = \tau(x)$$

where $y(x)$ and $\tau(x)$ are stochastic functions of the variable x. Let us characterize more precisely the statistical distribution of $y(x)$ and $\tau(x)$. For this, we assume momentarily that *there are no vertical barriers* or, more precisely, that we are only considering particle motions between successive collisions with vertical barriers. Then, if the (constant) vertical velocity is $\bar{V}_2 + 1$, we have

$$\frac{dy}{dx} = \frac{dy}{dt} \cdot \frac{dt}{dx}$$
$$= \frac{\bar{V}_2 + 1}{\bar{V}_1 \pm 1}$$

and the sign of the denominator depends on which horizontal layer the point (x, y) is located. As x increases, the particle travels in the positive x and y directions (we suppressed the vertical barriers). Therefore, since $\{Y_l\}$ is a Markov process, dy/dx is a two-state Markov process with states

$$w_+ = \frac{\bar{V}_2 + 1}{\bar{V}_1 + 1}, \qquad w_- = \frac{\bar{V}_2 + 1}{\bar{V}_1 - 1}$$

The jump rates associated to each state are obtained by observing that if $dy/dx = (\bar{V}_2 + 1)/(\bar{V}_1 + 1)$ for a "duration" δx, then

$$\delta y = \frac{\bar{V}_2 + 1}{\bar{V}_1 + 1} \delta x \tag{27}$$

where δy is the separation between successive horizontal barriers. This separation is exponentially distributed with mean 1; and we deduce that the corresponding rate is

$$r_+ = \frac{\bar{V}_2 + 1}{\bar{V}_1 + 1}$$

Similarly, the rate corresponding to w_- is

$$r_- = \frac{\bar{V}_2 + 1}{\bar{V}_1 - 1}$$

This determines completely the Markov process *dy/dx inside a vertical layer with vertical velocity* $\bar{V}_2 + 1$. What happens after collision with a vertical barrier? Clearly, since the vertical velocity changes to $\bar{V}_2 - 1$, the above description should be changed. Note, however, that, the derivative process dy/dx in the new vertical layer is again Markovian, with states

$$w_+ = \frac{\bar{V}_2 - 1}{\bar{V}_1 + 1} \quad \text{and} \quad w_- = \frac{\bar{V}_2 - 1}{\bar{V}_1 - 1}$$

and respective rates

$$r_+ = \frac{|\bar{V}_2 - 1|}{\bar{V}_1 + 1} \quad \text{and} \quad r_- = \frac{|\bar{V}_2 - 1|}{\bar{V}_1 - 1} \tag{28}$$

A key observation for obtaining a global representation for dy/dx *valid across all vertical barriers* is the following: Let $w(s)$ be a two-state Markov process with states

$$w_+ = \frac{1}{\bar{V}_1 + 1}, \qquad w_- = \frac{1}{\bar{V}_1 - 1}$$

and respective jump rates

$$r_+ = \frac{1}{\bar{V}_1 + 1}, \qquad r_- = \frac{1}{\bar{V}_1 - 1}$$

Then, if the origin is contained in a vertical layer with velocity $\bar{V}_2 + 1$, we can represent dy/dx, before collision with the first vertical barrier, as

$$\frac{dy}{dx}(x) = (\bar{V}_2 + 1)\, w((\bar{V}_2 + 1)\, x)$$

and thus

$$y(x) = (\bar{V}_2 + 1) \int_0^x w((\bar{V}_2 + 1)\, s)\, ds \tag{29}$$

Let $x = X_1$ denote the position of the first vertical barrier. Then, for $X_1 \leqslant x < X_2$, we have

$$y(x) = y(X_1) + (\bar{V}_2 - 1) \int_0^{x - X_1} w((\bar{V}_2 - 1)\, s + (\bar{V}_2 + 1)\, X_1)\, ds \tag{30}$$

in terms of the *same* basic process $w(s)$. For $\bar{V}_2 - 1 > 0$, this follows from the fact that $\{Y_t\}$ is Markovian. For $\bar{V}_2 - 1 < 0$, Eq. (30) states that the

path has been "reflected" about $x = X_1$ and revisits the same horizontal layers. A moment of thought reveals that the jumps in dy/dx, according to Eq. (30), occur exactly at the horizontal barriers determined by $\{Y_l\}$—as they should.

This argument shows that the total y displacement after two collisions is given by

$$\Delta y_1 = (\bar{V}_2 + 1) \int_0^{\Delta x_1} w((\bar{V}_2 + 1)\, s)\, ds + (\bar{V}_2 - 1)$$

$$\times \int_0^{\Delta x_2} w((\bar{V}_2 - 1)\, s + (\bar{V}_2 + 1)\, \Delta x_1)\, ds \tag{31}$$

with $\Delta x_1 = X_1 - 0$ and $\Delta x_2 = X_2 - X_1$. Analogously, the *time* elapsed up to the second vertical collision is given by

$$\Delta \tau = \int_0^{\Delta x_1} w((\bar{V}_2 + 1)\, s)\, ds + \int_0^{\Delta x_2} w((\bar{V}_2 - 1)\, s + (\bar{V}_2 + 1)\, \Delta x_1)\, ds \tag{32}$$

This equation follows from (29), (30), and $\delta y/\delta t = \bar{V}_2 \pm 1$, where the sign depends on the vertical layer.

More generally, the above method allows for a representation of the functions $y(x)$ and $\tau(x)$ for all $x > 0$, in terms of a single two-state process $w(s)$ which depends only on $\{Y_l\}$, and of the positions of the vertical barriers $\{x = X_n\}$, $n = 1, 2, 3, \ldots$. Of special interest to us are the *successive increments* Δy_n and $\Delta \tau_n$, after $2n$ collisions, for $n = 1, 2, 3, \ldots$. To derive a convenient representation for these increments, we write

$$\begin{aligned} \alpha &= \bar{V}_2 + 1 \\ \beta &= \bar{V}_2 - 1 \end{aligned} \tag{32'}$$

and

$$p_i = \Delta x_{2i-1} = X_{2i-1} - X_{2i-2}$$

$$q_i = \Delta x_{2i} = X_{2i} - X_{2i-1}$$

for $i = 1, 2, 3, \ldots$. We also set

$$A_n = \sum_{i=1}^{n} (\alpha p_i + \beta q_i), \qquad n \geqslant 1$$

With these notations, the increment Δy_n corresponding to the interval $X_{2n-2} \leqslant x \leqslant X_{2n}$ is

$$\Delta y_n = (\bar{V}_2 + 1) \int_0^{p_n} w(\alpha s + A_{n-1})\, ds$$

$$+ (\bar{V}_2 - 1) \int_0^{q_n} w(\beta s + A_{n-1} + \alpha p_n)\, ds \tag{33}$$

Similarly, the time elapsed between the $2(n-1)$th and $2n$th collisions is

$$\Delta\tau_n = \int_0^{p_n} w(\alpha s + A_{n-1})\, ds + \int_0^{q_n} w(\beta s + A_{n-1} + \alpha p_n)\, ds \tag{34}$$

To obtain these formulas, we simply applied repeatedly the method used to calculate Δy_1 and $\Delta\tau_1$. These representation formulas for the increments are the basis of the calculations of the mean-square displacements. The increments of space and time Δ_{yk} and $\Delta\tau_k$ measure the path fluctuations within a *correlation length* of the random velocity. To compute the long-time/large-distance mean-square displacements, we must calculate the correlations between the pairs Δy_k, Δy_l and $\Delta\tau_k$, $\Delta\tau_l$ for $|k-l| = 0$, 1, 2, 3,..., etc.; i.e., the correlations of the path on scales larger than the velocity correlation length. Notice that since $w(s)$ is statistically translation invariant, the random variables $\Delta y_1, \Delta y_2, \ldots$, and $\Delta\tau_1, \Delta\tau_2, \ldots$, form stationary sequences.

It is readily found that

$$\begin{aligned} \lim_{t\to\infty} \frac{1}{2t^{\nu}} \langle [x(t) - \bar{V}_1 t]^2 \rangle &= \lim_{n\to} \frac{\langle [X_n - \bar{V}_1 \tau(X_n)]^2 \rangle}{2\langle \tau(X_n) \rangle^{\nu}}, \quad \nu = 1 \text{ or } \frac{3}{2} \\ \lim_{t\to\infty} \frac{1}{2t} \langle [y(t) - \bar{V}_2 t]^2 \rangle &= \lim_{n\to\infty} \frac{\langle [y(X_n) - \bar{V}_2 \tau(X_n)]^2 \rangle}{2\langle \tau(X_n) \rangle} \end{aligned} \tag{34'}$$

In words, the $t \to \infty$ asymptotics can be obtained by taking the limit along the sequence of (Markov) stopping times $\tau(X_n)$, $n = 1, 2, 3, \ldots$. The random variable $X_n - \bar{V}_1 \tau(X_n)$ can be written in the form

$$\begin{aligned} X_n - \bar{V}_1 \tau(X_n) &= \sum_{j=1}^{n} [p_j + q_j - \bar{V}_1 \Delta\tau_j] \\ &= \sum_{j=1}^{n} \left[\int_0^{p_j} z(\alpha s + A_{j-1})\, ds + \int_0^{q_j} z(\beta s + A_{j-1} + \alpha p_j)\, ds \right] \end{aligned} \tag{35}$$

where

$$z(s) = 1 - \bar{V}_1 w(s) \tag{36}$$

To obtain formula (35), we used the characterization of $\Delta\tau_j$ in (34). A similar computation using (33) and (34) gives

$$\begin{aligned} y(X_n) - \bar{V}_2 \tau(X_n) = \sum_{j=1}^{n} \Bigg[& \int_0^{p_j} w(\alpha s + A_{j-1})\, ds \\ & - \int_0^{q_j} w(\beta s + A_{j-1} + \alpha p_j)\, ds \Bigg] \end{aligned} \tag{37}$$

For simplicity, we set

$$\xi_j \equiv \int_0^{p_j} z(\alpha s + A_{j-1})\, ds + \int_0^{q_j} z(\beta s + A_{j-1} + \alpha p_j)\, ds \tag{38}$$

and

$$\eta_j \equiv \int_0^{p_j} w(\alpha s + A_{j-1})\, ds - \int_0^{q_j} w(\beta s + A_{j-1} + \alpha p_j)\, ds \tag{39}$$

Using the stationarity of Δy_j, $\Delta \tau_j$, the second moments of $X_n - \bar{V}_1 \tau(X_n)$ and $y(X_n) - \bar{V}_2 \tau(X_n)$ can be expressed as follows:

$$\langle [X_n - \bar{V}_1 \tau(X_n)]^2 \rangle = n\langle \xi_1^2 \rangle + 2 \sum_{j=2}^{n} (n-j+1)\langle \xi_1 \xi_j \rangle \tag{40}$$

and

$$\langle [y(X_n) - \bar{V}_2 \tau(X_n)]^2 \rangle = n\langle \eta_1^2 \rangle + 2 \sum_{j=2}^{n} (n-j+1)\langle \eta_1 \eta_j \rangle \tag{41}$$

Note that, from (34), we have

$$\tau(X_n) = \sum_{j=1}^{n} \left[\int_0^{p_j} w(\alpha s + A_{j-1})\, ds + \int_0^{q_j} w(\beta s + A_{j-1} + \alpha p_j)\, ds \right]$$

and, since $w(s)$ and $\{X_k\}$ are independent and $w(s)$ is translation invariant, the mean of $\tau(X_n)$ is

$$\begin{aligned} \langle \tau(X_n) \rangle &= n(\langle p_j \rangle + \langle q_j \rangle)\langle w(0) \rangle \\ &= \frac{2n}{\bar{V}_1} \end{aligned} \tag{42}$$

In deriving this last equation, we used the explicit value for the mean of $w(0)$,

$$\begin{aligned} \langle w(0) \rangle &= (r_+ w_- + r_- w_+)/(r_+ + r_-) \\ &= 1/\bar{V}_1 \end{aligned}$$

and the fact that p_j, q_j have mean 1.

To compute the correlations $\langle \xi_1 \xi_j \rangle$ and $\langle \eta_1 \eta_j \rangle$ for $j = 0, 1, 2, 3, \ldots$, we observe first that the covariances of the processes $w(s)$ and $z(s)$ can be evaluated explicitly, and are given by

$$\langle w(s)\, w(s')\rangle = \frac{1}{\bar{V}_1^2} + \frac{1}{\bar{V}_1^2(\bar{V}_1^2-1)} \exp\left[-\frac{2\bar{V}_1}{(\bar{V}_1^2-1)} |s-s'| \right]$$
$$= \frac{1}{\bar{V}_1^2} + K \exp(-R\,|s-s'|)$$
$$\equiv \rho_w(s-s') \tag{43}$$

and

$$\langle z(s)\, z(s')\rangle = \frac{1}{\bar{V}_1^2-1} \exp\left[-\frac{2\bar{V}_1}{(\bar{V}_1^2-1)} |s-s'| \right]$$
$$= Q \exp(-R\,|s-s'|)$$
$$\equiv \rho_z(s-s') \tag{44}$$

These formulas follow from the theory of continuous-time Markov processes with finite state space (see Baht,[22] Chapter 9; and Appendix B herein). Using these covariances, we can evaluate the autocorrelation functions of $\{\xi_j\}$ and $\{\eta_j\}$ by taking the expectation of the products $\xi_1\xi_j$, $\eta_1\eta_j$ *first with respect to z and w*, i.e., the $\{Y_l\}$ statistics, and subsequently averaging over p_j, q_j, $j=1, 2,...$, (the $\{X_k\}$ statistics). In this way, we obtain

$$\langle \xi_1^2 \rangle = \left\langle \left(\int_0^{p_1} z(\alpha s)\, ds + \int_0^{q_1} z(\beta s + \alpha p_1)\, ds \right)^2 \right\rangle$$
$$= \left\langle \int_0^{p_1}\int_0^{p_1} \rho_z(\alpha(s-s'))\, ds\, ds' \right\rangle$$
$$+ \left\langle \int_0^{q_1}\int_0^{q_1} \rho_z(\beta(s-s'))\, ds\, ds' \right\rangle$$
$$+ 2\left\langle \int_0^{p_1}\int_0^{q_1} \rho_z(\alpha s - \beta s' - \alpha p_1)\, ds\, ds' \right\rangle \tag{45}$$

and, for $n \geqslant 2$,

$$\langle \xi_1 \xi_n \rangle = \left\langle \int_0^{p_1}\int_0^{p_n} \rho_z(\alpha s - \alpha s' - A_{n-1})\, ds\, ds' \right\rangle$$
$$+ \left\langle \int_0^{p_1}\int_0^{q_n} \rho_z(\alpha s - \beta s' - A_{n-1} - \alpha p_n)\, ds\, ds' \right\rangle$$
$$+ \left\langle \int_0^{q_1}\int_0^{p_n} \rho_z(\beta s - \alpha p_1 - \alpha s' - A_{n-1})\, ds\, ds' \right\rangle$$
$$+ \left\langle \int_0^{q_1}\int_0^{q_n} \rho_z(\beta s + \alpha p_1 - \beta s' - A_{n-1} - \alpha p_n)\, ds\, ds' \right\rangle \tag{46}$$

The expressions for $\langle \eta_1^2 \rangle$ and $\langle \eta_1 \eta_n \rangle$ are similar, with ρ_w instead of ρ_z and with negative signs in front of the "mixed" terms $\langle \int_0^{p_1} \int_0^{q_n} \rho_w \rangle$ and $\langle \int_0^{q_1} \int_0^{p_n} \rho_w \rangle$, due to the minus sign appearing in the definition of η_n in (39). The resulting formulas can be further reduced by computing explicitly the expectations over p_i, q_j. In Appendix B, we show that evaluation of the expectations with respect to p_i, q_j leads to the following expressions:

$$\langle \xi_1^2 \rangle = 2Q \left(\frac{2\alpha - \beta}{\alpha - \beta} \frac{1}{1 + R\alpha} + \frac{2\beta - \alpha}{\beta - \alpha} \frac{1}{1 + R|\beta|} \right) \tag{47}$$

$$\langle \xi_1 \xi_n \rangle = \frac{Q}{\pi} \int_{-\infty}^{+\infty} \frac{R\, dk}{R^2 + k^2} \frac{4 + 2i(\alpha + \beta)\, k - \alpha\beta k^2}{(1 + i\alpha k)^n (1 + i\beta k)^n}, \quad n \geqslant 2 \tag{48}$$

$$\langle \eta_1^2 \rangle = \frac{2}{\bar{V}_1^2} + 2K \left(\frac{\beta}{\beta - \alpha} \frac{1}{1 + R\alpha} + \frac{\alpha}{\alpha - \beta} \frac{1}{1 + R|\beta|} \right) \tag{49}$$

and

$$\langle \eta_1 \eta_n \rangle = \frac{K}{\pi} \int_{-\infty}^{+\infty} \frac{R\, dk}{R^2 + k^2} \frac{\alpha\beta k^2}{(1 + i\alpha k)^n (1 + i\beta k)^n} \tag{50}$$

for $n \geqslant 2$. The constants α, β, R, K, Q are simple functions of $\bar{V}_1$ and $\bar{V}_2$; cf. (32′), (43), and (44). Notice that, from (48) and (50), the autocorrelation coefficients $\langle \xi_1 \xi_n \rangle$, $\langle \eta_1 \eta_n \rangle$ have a similar structure.

A closer inspection shows that, for all α and β, the series $\sum_2^\infty \langle \eta_1 \eta_n \rangle$ converges absolutely and

$$\sum_{n=2}^{\infty} \langle \eta_1 \eta_n \rangle = \frac{K}{\pi} \int_{-\infty}^{+\infty} \frac{R\, dk}{R^2 + k^2} \times \frac{\alpha\beta k^2}{(1 + ik\alpha)(1 + ik\beta)[i(\alpha + \beta)\, k - \alpha\beta k^2]} \tag{51}$$

This expression is obtained by summing the coefficients (50) by interchanging the order of summation and integration, and using the formula

$$\sum_{n=2}^{\infty} \frac{1}{(1 + i\alpha k)^n (1 + i\beta k)^n} = \frac{1}{(1 + i\alpha k)(1 + i\beta k)[i(\alpha + \beta)\, k - \alpha\beta k^2]}$$

The integral in (51) can be evaluated explicitly. Noting that, from (40),

$$\lim_{n\to\infty}\frac{1}{n}\left\langle\left(\sum_{j=1}^{n}\eta_j\right)^2\right\rangle=\langle\eta_1^2\rangle+2\sum_{j=2}^{\infty}\langle\eta_1\eta_j\rangle$$

and using the expression for the series calculated from (51) given in Appendix B, we obtain

$$\lim_{n\to\infty}\frac{1}{n}\left\langle\left|\sum_{j=1}^{n}\eta_j\right|^2\right\rangle = \frac{2}{(\bar V_1)^2}\left(1+\frac{|\bar V_2|}{|\bar V_2|\cdot|\bar V_1^2-1|+|\bar V_1|\cdot|\bar V_2^2-1|}\right)$$

The dimensionless effective diffusivity D_{22}^* is obtained by dividing by $2\times(2/\bar V_1)$, according to (34′) and (42). Therefore, we have

$$D_{22}^*=\frac{1}{2|\bar V_1|}\left(1+\frac{|\bar V_2|}{|\bar V_2|\cdot|\bar V_1^2-1|+|\bar V_1|\cdot|\bar V_2^2-1|}\right) \tag{52}$$

The diffusivity $D_\perp^*$ is obtained by setting $\bar V_2=0$ in this equation. Finally, the dimensional expressions for D_{22}^* and $D_\perp^*$ in (24) and (24′) follow from this formula by restoring units.

Next, we turn to the evaluation of the second moment $\langle|\sum_1^n\xi_j|^2\rangle$. Summation of the series $\sum_j\langle\xi_1\xi_j\rangle$ with the above method of interchanging sum and integral leads, formally, to

$$\sum_{j=2}^{\infty}\langle\xi_1\xi_j\rangle=\frac{Q}{\pi}\int_{-\infty}^{+\infty}\frac{R\,dk}{R^2+k^2} \times\frac{4+2i(\alpha+\beta)k-\alpha\beta k^2}{(1+i\alpha k)(1+i\beta k)[i(\alpha+\beta)k-\alpha\beta k^2]} \tag{53}$$

We distinguish two cases: $\alpha+\beta=0$ and $\alpha+\beta\neq0$. If $\alpha+\beta(=2\bar V_2)=0$, then $\alpha=1$, $\beta=-1$; this corresponds to the parallel-resonant case. In the latter case the integrand in (53) is

$$\frac{R}{R^2+k^2}\,\frac{4+k^2}{k^2(1+k^2)}$$

It behaves like $1/k^2$ for $k\ll1$ and hence the integral diverges. This $O(k^{-2})$ infrared divergence reflects the fact that *the motion of the x coordinate is*

superdiffusive in the parallel-resonant case, and thus $\nu = 1$ is not the appropriate exponent. The decay of correlations can be estimated precisely from the formula (48): In fact,

$$\begin{aligned}\langle \xi_1 \xi_n \rangle &= \frac{Q}{\pi} \int_{-\infty}^{+\infty} \frac{R\,dk}{R^2 + k^2} \frac{4 + k^2}{(1 + k^2)^n} \\ &= \frac{1}{\sqrt{n}} \frac{Q}{\pi} \int_{-\infty}^{+\infty} \frac{R\,dk}{R^2 + (k/\sqrt{n})^2} \frac{4 + (k/\sqrt{n})^2}{(1 + k^2/n)^n} \\ &\sim \frac{4}{\sqrt{n}} \frac{Q}{R\pi} \int_{-\infty}^{+\infty} e^{-k^2}\,dk \\ &= \frac{4}{\sqrt{n}} \frac{Q}{R\sqrt{\pi}} = \frac{1}{\sqrt{n}} \left(\frac{2}{\bar{V}_1 \sqrt{\pi}} \right)\end{aligned}$$

Therefore, the second moment $\langle (\sum \xi_j)^2 \rangle$ grows like $\sum_{k=1}^{n} \sum_{j=1}^{n} |k-j|^{-1/2} = O(n^{3/2})$, and the longitudinal displacements are superdiffusive ($\nu = 3/2$). Using (47) and (48), we can actually compute the asymptotic mean-square displacement exactly. In fact,

$$\frac{1}{n^{3/2}} \left\langle \left(\sum_{j=1}^{n} \xi_j \right)^2 \right\rangle = \frac{1}{\sqrt{n}} \langle \xi_1^2 \rangle + \frac{2}{n^{3/2}} \sum_{j=2}^{n} (n - j + 1) \langle \xi_1 \xi_j \rangle \tag{54}$$

The first term is negligible as $n \to \infty$. The last one can be written in the form

$$\begin{aligned}&\frac{2Q}{\pi n^{3/2}} \int_{-\infty}^{+\infty} \left[\sum_{j=2}^{n} (n - j + 1) \frac{4 + k^2}{(1 + k^2)^j} \right] \\ &\quad = \frac{2Q}{\pi} \int_{-\infty}^{+\infty} \frac{R\,dk}{R^2 + k^2/n} \left[\frac{1}{n} \sum_{j=2}^{n} \left(1 - \frac{j-1}{n} \right) \frac{4 + (k^2/n)}{(1 + k^2/n)^j} \right]\end{aligned} \tag{55}$$

Since, for $j/n \simeq x$, $n \to \infty$,

$$(1 + k^2/n)^j \simeq e^{k^2 x}$$

the term in brackets in (55) can be regarded as a Riemann sum approximating the integral

$$4 \int_0^1 (1 - x)\, e^{-xk^2}\,dx$$

Substituting in (54), we conclude that

$$\lim_{n\to\infty}\frac{1}{n^{3/2}}\left\langle\left(\sum\xi_j\right)^2\right\rangle=\frac{8Q}{\pi}\int_{-\infty}^{+\infty}\frac{dk}{R}\int_0^1(1-x)\,e^{-xk^2}\,dx$$
$$=\frac{8Q}{R\sqrt{\pi}}\int_0^1\frac{1-x}{\sqrt{x}}\,dx$$
$$=\frac{32Q}{3R\sqrt{\pi}}$$
$$=\frac{16}{3\bar{V}_1\sqrt{\pi}} \tag{56}$$

To obtain the asymptotic result in real time, we use $\langle\tau_n\rangle\sim 2n/\bar{V}_1$. Multiplying (56) by $(\bar{V}_1/2)^{3/2}$, we obtain, in dimensionless variables,

$$\lim_{n\to\infty}\frac{[x(t)-\bar{V}_1 t]^2}{t^{3/2}}=\left[\frac{4}{3}\left(\frac{2}{\pi}\right)^{1/2}\right]|\bar{V}_1|^{1/2}$$

The dimensional result (25) follows by restoring units, $t\to ta/\bar{U}$, $x\to ax$, $\bar{V}_1\to\bar{V}_1\bar{U}$.

Finally, if $\alpha+\beta=2\bar{V}_2\neq 0$, the series $\sum_{j=2}^{\infty}\langle\xi_1\xi_j\rangle$ is absolutely convergent and its sum is given by the integral (53). In Appendix B we evaluate explicitly this sum in terms of Q, R, α, and β. Using the expression for the variance in (40) and the explicit evaluation of the integral, we conclude that

$$\lim_{n\to\infty}\frac{\langle[X_n-\bar{V}_1\tau(X)]^2\rangle}{n}=\frac{2}{|\bar{V}_1|\cdot|\bar{V}_2|}$$
$$\times\left(1+\frac{|\bar{V}_1|}{|\bar{V}_1|\cdot|\bar{V}_2^2-1|+|\bar{V}_2|\cdot|\bar{V}_1^2-1|}\right)$$

The dimensionless diffusivity D_{11}^* can be computed by dividing by $2\langle\tau_1\rangle\sim 2\times 2/|V_1|$. We obtain, accordingly,

$$D_{11}^*=\frac{1}{2\,|\bar{V}_2|}\left(1+\frac{|\bar{V}_1|}{|\bar{V}_1|\cdot|\bar{V}_2^2-1|+|\bar{V}_2|\cdot|\bar{V}_1^2-1|}\right)$$

and the final result (23) is obtained by restoring dimensions.

This concludes the proof of Theorem 5. ■

Remarks. 1. *The parallel-resonant case.* The relation found between the asymptotic mean-square displacements of the x and y coordinates

$$\frac{\langle [y(t)]^2 \rangle}{t} \sim 2D_\perp^*$$

$$\frac{\langle [\delta x(t)]^2 \rangle}{t^{3/2}} \sim \frac{a\bar{U}^2}{(2D_\perp^*)^{1/2}} \left[\frac{4}{3} \left(\frac{2}{\pi} \right)^{1/2} \right]$$

is identical to the one in the Matheron and de Marsily (MdM) model[7]; see, in particular, Zumofen *et al.*[17] The difference between MdM and the present situation is that in the former, the particle is undergoing advection-diffusion in a stratified medium, driven by a Brownian motion (molecular diffusion) which is independent of the velocity statistics. In the present model there is no molecular diffusion; nevertheless the particle experiences an "effective" transverse diffusion through multiple collisions with the vertical barriers. Therefore, the situation is similar to the so-called "nearly-stratified" models discussed by Avellaneda and Majda,[16] in which it is shown how the small-scale features of a perturbed stratified flow contribute to the transverse effective diffusivity on the one hand, and how the infrared portion of the spectrum of the velocity gives rise to anomalous diffusion with $\nu = 3/2$. On the scale of the wider horizontal layers, the system behaves effectively like the MdM model. This point is discussed in more detail below (Section 4.3).

2. *The diagonal-resonant case.* Expansion of the effective diffusivities D_{11}^* and D_{22}^* in the vicinity of $|\bar{V}_1| = \bar{U}$, $|\bar{V}_2| = |\bar{U}|$ shows that, to leading order,

$$D_{ii}^* \sim \frac{a\bar{U}^2}{4(||\bar{V}_1| - |\bar{U}|| + ||\bar{V}_2| - |\bar{U}||)} \tag{57}$$

and hence that D_{ii}^* diverge near the resonant values. As mentioned earlier, this is due to the disparity of particle motions according to whether they originate at a nearly "stagnant" cell or not. From the point of view of the piston-flow model, the existence of stagnation cells distributed throughout the medium gives rise to a very wide mixing region characterized by D_{ii}^* in (57). This is well confirmed by numerical simulations (see Section 5).

3. *The case* $\rho = 1$, $|\bar{V}_1| \neq \bar{U}$, *or* $|\bar{V}_2| \neq \bar{U}$. The proof of Theorem 5 applies only to mean velocities with $\rho > 1$. However, the methods of proof extend to the regimes $|\bar{V}_1| = \bar{U}$, $|\bar{V}_2| < \bar{U}$, or vice versa, since time is still a monotone (but discontinuous) function of x or y. Using a similar Markovian argument, it can be verified that D_{11}^* and D_{22}^* are continuous up

to the edges of the subcritical box (depicted in Fig. 1), except in a vicinity of the diagonal resonance.

4. *The Markovianization.* This technique for establishing diffusive behavior for equations of type (1) was first introduced by Kesten and Papanicolaou.[23] These authors studied the case $|\bar{\mathbf{V}}| \gg \bar{U}$ (infinite mean-to-fluctuations ratio) for more general velocity fluctuations; they established rigorously the validity of the Kubo approximation in this limit.

4.2. Asymptotic Probability Distribution for $\bar{V}_1 \cdot \bar{V}_2 \neq 0$

We have shown above that the stochastic processes $y(X_n) - \bar{V}_2 \tau(X_n)$, $n \geqslant 0$, and $X_n - \bar{V}_1 \tau(X_n)$ admit a Markovian representation in terms of the two-state process $w(s)$ depending on $\{Y_l\}$, and the Poisson process $\{X_k\}$. In the case $\bar{V}_1 \bar{V}_2 \neq 0$, the asymptotic mean-square displacements are Fickian ($\nu = 1$). This raises the question of characterizing the asymptotic distribution of the fluctuations which are expected to be normally distributed. Here, we shall not give a complete proof of the asymptotic normality of $(1/\sqrt{t})[x(t) - \bar{V}_1 t]$ and $(1/\sqrt{t})[y(t) - \bar{V}_2 t]$, but only point out the main ingredient in the proof of this result.[21] In fact, from the representations for $X_n - \bar{V}_1 \tau(X_n)$ and $y(X_n) - \bar{V}_2 \tau(X_n)$ obtained in the proof of Theorem 5, we note that these stochastic processes can be viewed as Markov processes which are *functions of the strongly mixing processes* $\{X_k\}$, $\{Y_l\}$, in the sense of Ibragimov[24] and Billingsley (ref. 25, Chapter 4). A deeper analysis along these lines allows us to apply a suitable form of the Central Limit Theorem to conclude that the fluctuations are indeed normally distributed. Asymptotic normality is confirmed clearly by the Monte Carlo simulations (Section 5).

4.3. Asymptotic Distributions in the Parallel-Resonant Case ($\bar{V}_1 \cdot \bar{V}_2 = 0$)

A crucial property of the model for characterizing the asymptotic distribution of

$$\frac{1}{t^{3/4}} [x(t) - \bar{V}_1 t], \qquad t \gg 1$$

is that, if $|\bar{V}_1| > \bar{U}$ and $\bar{V}_2 = 0$, then the process $y(t)/\sqrt{t}$ "thermalizes" to a Gaussian distribution with variance $2D_\perp^*$, *conditionally* with respect to the distribution of the Poisson barriers $\{Y_l\}$. Simply put, the asymptotic distribution of $y(t)/\sqrt{t}$ is seld-averaging with respect to $\{\mathbf{Y}_l\}$. This is expressed precisely in the following result.

Proposition 6. If $|\bar{V}_1| > \bar{U}$ and $\bar{V}_2 = 0$, then the paths $\{y_\varepsilon(t), 0 \leqslant t \leqslant 1\}$, $\varepsilon > 0$, defined by

$$y_\varepsilon(t) = \varepsilon y\left(\frac{t}{\varepsilon^2}\right), \qquad 0 \leqslant t \leqslant 1, \quad \varepsilon > 0$$

converge in distribution as $\varepsilon \to 0$ to a Wiener process $\{(2D_\perp^*)^{1/2}\beta(t), 0 \leqslant t \leqslant 1\}$, conditionally on $\{Y_l\}$. Specifically, let $\Phi[y(\cdot)]$ be an arbitrary, continuous functional in path space and let $\langle \cdot | \{Y_l\} \rangle$ denote conditional expectation with respect to $\{Y_l\}$. Then,

$$\lim_{\varepsilon \to 0} \langle \Phi[y_\varepsilon(\cdot)] \mid \{Y_l\} \rangle = E\{\Phi[(2D_\perp^*)^{1/2}\beta(\cdot)]\} \tag{58}$$

where $E\{\cdot\}$ denotes integration with respect to the Brownian path $\beta(t)$, $0 \leqslant t \leqslant 1$.

Proof. We use dimensionless variables for simplicity. The representation for η_j obtained in (39) gives for $\alpha = 1, \beta = -1$ (corresponding to $\bar{V}_2 = 0$)

$$\eta_j = \int_0^{p_j} w(s + A_{j-1})\, ds - \int_0^{q_j} w(-s + A_{j-1} + p_j)\, ds$$

$$= \int_{A_{j-1}}^{A_j} w(s)\, ds$$

Consequently, for all $m > 0$, we have

$$\begin{aligned} y(X_m) &= \sum_{j=1}^{m} \eta_j \\ &= \sum_{j=1}^{m} \int_{A_{j-1}}^{A_j} w(s)\, ds \\ &= \int_0^{A_m} w(s)\, ds \end{aligned} \tag{59}$$

We conclude from this that, for all $0 \leqslant t \leqslant 1$,

$$\frac{y(X_{[nt]})}{\sqrt{n}} = \frac{1}{\sqrt{n}} \int_0^{A_{[nt]}} w(s)\, ds$$

where $[x]$ = integer part of x. Decomposing $w(s)$ into its mean and fluctuating parts, $w(s) = \langle w \rangle + w'(s)$, we have

$$\frac{y(X_{[nt]})}{\sqrt{n}} = \langle w \rangle \frac{A_{[nt]}}{\sqrt{n}} + \frac{1}{\sqrt{n}} \int_0^{A_{[nt]}} w'(s)\, ds \tag{60}$$

The first summand is a normalized sum of independent random variables. Therefore, by Donsker's invariance principle,[25] $\langle w \rangle A_{[nt]}/\sqrt{n}$ converges in distribution to a Wiener process with mean zero and variance

$$\sigma^2 = \langle w \rangle^2 \langle (p_1 - q_1)^2 \rangle = \frac{2}{\bar{V}_1^2}$$

Hence, the corresponding diffusivity $D_\perp^*$ is

$$D_\perp^* = \frac{\sigma^2}{2\langle \tau_1 \rangle} = \frac{2/\bar{V}_1^2}{4/\bar{V}_1} = \frac{1}{2\bar{V}_1}$$

as calculated previously. It remains to show that the second term in (60),

$$\frac{1}{\sqrt{n}} \int_0^{A_{[nt]}} w'(s)\, ds$$

converges to zero in probability. In fact

$$\text{Prob}\left\{\left|\frac{1}{\sqrt{n}} \int_0^{A_{[nt]}} w'(s)\, ds\right| > \alpha\right\}$$

$$= \sum_{k=-\infty}^{+\infty} \text{Prob}\left\{\frac{1}{\sqrt{n}}\left|\int_0^{A_{[nt]}} w'(s)\, ds\right| > \alpha;\ \theta k \leqslant \frac{A_{[nt]}}{\sqrt{n}} < \theta(k+1)\right\} \qquad (61)$$

where θ is an arbitrary positive constant. If $\theta k \leqslant A_{[nt]}/\sqrt{n} < \theta(k+1)$, then

$$\left|\frac{1}{\sqrt{n}} \int_0^{A_{[nt]}} w'(s)\, ds - \frac{1}{\sqrt{n}} \int_0^{\theta k \sqrt{n}} w'(s)\, ds\right|$$

$$\leqslant \theta \cdot \max_s |w'(s)|$$

$$= \theta \cdot \max\left\{\frac{1}{\bar{V}_1 - 1} - \frac{1}{\bar{V}_1}, \frac{1}{\bar{V}_1} - \frac{1}{\bar{V}_1 + 1}\right\}$$

Therefore, for given $\alpha > 0$, if θ is chosen sufficiently small, we have

$$\left|\frac{1}{\sqrt{n}} \int_0^{A_{[nt]}} w'(s)\, ds - \frac{1}{\sqrt{n}} \int_0^{\theta k \sqrt{n}} w'(s)\, ds\right| \leqslant \frac{\alpha}{2}$$

for k such that $\theta k \sqrt{n} \leqslant A_{[nt]} < \theta(k+1)\sqrt{n}$. Because of this, using (61), we obtain

$$\begin{aligned}
&\text{Prob}\left\{\left|\frac{1}{\sqrt{n}}\int_0^{A_{[nt]}} w'(s)\,ds\right| > \alpha\right\} \\
&\quad \leqslant \sum_{k=-\infty}^{+\infty} \text{Prob}\left\{\left|\frac{1}{\sqrt{n}}\int_0^{\theta k\sqrt{n}} w'(s)\,ds\right| > \frac{\alpha}{2};\ \theta k \leqslant \frac{A_{[nt]}}{\sqrt{n}} < \theta(k+1)\right\} \\
&\quad = \sum_{k=-\infty}^{+\infty} \text{Prob}\left\{\left|\frac{1}{\sqrt{n}}\int_0^{\theta k\sqrt{n}} w'(s)\,ds\right| > \frac{\alpha}{2}\right\} \\
&\qquad \times \text{Prob}\left\{\theta k \leqslant \frac{A_{[nt]}}{\sqrt{n}} < \theta(k+1)\right\} \qquad (62)
\end{aligned}$$

In this last equality we made use of the independence of $w'(s)$ and A_n. Now, by the Ergodic Theorem, we have

$$\lim_{n\to\infty} \Pr\left\{\left|\frac{1}{\sqrt{n}}\int_0^{\theta k\sqrt{n}} w'(s)\,ds\right| > \frac{\alpha}{2}\right\} = 0$$

for all integers k. Therefore, all the summands of the series in (62) converge to zero. The convergence of the entire sum to zero follows from the estimate

$$\begin{aligned}
\sum_{|k|>M} \text{Prob}\left\{\theta k \leqslant \frac{A_{[nt]}}{\sqrt{n}} < \theta(k+1)\right\} &\leqslant \text{Prob}\left\{\left|\frac{A_{[nt]}}{\sqrt{n}}\right| > \theta(M-1)\right\} \\
&\approx e^{-\theta^2(M-1)^2/2\sigma^2}, \qquad n \gg 1
\end{aligned}$$

which shows that the tail sums in (62) can be made uniformly small by taking M large enough.

The *conditional convergence* of $y(t)/\sqrt{t}$ to $(2D_\perp^*)^{1/2}\,\beta(t)$ in the sense of (58) follows, since we have established that

$$\frac{y(X_{[nt]})}{\sqrt{n}} = F(t) + G(t) \qquad (63)$$

where $F(t)$ depends only on the Poisson process $\{X_k\}$ and converges to $(2D_\perp^*)^{1/2}\,\beta(t)$ in distribution, and the remainder $G(t)$ converges to zero in probability. ■

We now give a sketch of the characterization of the asymptotic distribution of

$$\frac{\delta x(t)}{t^{3/4}} \equiv \frac{1}{t^{3/4}}\,[x(t) - \bar{V}_1 t] \qquad (64)$$

based on Proposition 6. From the basic equations of motion, we have

$$\frac{\delta x(t)}{t^{3/4}} = \frac{1}{t^{3/4}} \int_0^t U_1(y(s))\, ds$$

$$= t^{1/4} \int_0^1 U_1 \left[t^{1/2} \left(\frac{y(st)}{t^{1/2}} \right) \right] ds \tag{65}$$

We know from Proposition 6 that $y(st)/\sqrt{t}$ converges, *conditionally on* $\{Y_l\}$, to a Wiener process $(2D_\perp^*)^{1/2}\, \beta(s)$. Moreover, an elementary application of the Central Limit Theorem shows that the rescaled velocity in (65),

$$t^{1/4} U_1(t^{1/2} y)$$

which depends only on $\{Y_l\}$, converges in distribution to a Gaussian white noise $N(y)$ satisfying

$$\langle N(y) \rangle = 0$$

$$\langle N(y)\, N(y') \rangle = a\bar{U}^2 \delta(y - y')$$

Since $\{y(st)/\sqrt{t}\}$ converges conditionally on $\{Y_l\}$ to $(2D_\perp^*)^{1/2}\, \beta(s)$, $N(y)$ and $\beta(s)$ are necessarily statistically independent. Moreover, it can be shown that formal passage to the limit in (65) is justified, although this is mathematically subtle because $N(y)$ is not a continuous function of y.[21] Passage to the limit in (65) gives

$$\frac{\delta x(t)}{t^{3/4}} \sim \int_0^1 N((2D_\perp^*)^{1/2}\, \beta(s))\, ds, \qquad t \gg 1 \tag{66}$$

with $N(y)$ and $\beta(s)$ independent.

Using this result, we conclude the following result.

Theorem 7. The asymptotic probability density $\bar{P}(x)$ of $\delta x(t)/t^{3/4}$ has Fourier transform

$$\hat{\bar{P}}(k) = \mathbf{E} \left\{ \exp\left(-[k^2 a \bar{U}^2 / 2(2D_\perp^*)^{1/2}] \int_0^1 \int_0^1 \delta(\beta(s) - \beta(s'))\, ds\, ds' \right) \right\} \tag{67}$$

Proof. Using (66), we have

$$\hat{\bar{P}}(k) = \left\langle E \left\{ \exp\left[ik \int_0^1 N((2D_\perp^*)^{1/2}\, \beta(s))\, ds \right] \right\} \right\rangle$$

Taking the expectation with respect to the Gaussian white noise first, we obtain

$$\hat{\bar{P}}(k) = \mathbf{E}\left\{\exp\left(-(k^2 a\bar{U}^2/2)\int_0^1\int_0^1 \delta((2D_\perp^*)^{1/2}\,[\beta(s)-\beta(s')])\,ds\,ds'\right)\right\}$$

The result (67) follows by using the scaling relation $\delta((2D_\perp^*)^{1/2}\,y) = (2D_\perp^*)^{-1/2}\,\delta(y)$. ■

This characterizes the asymptotic distribution of $\delta x(t)/t^{3/4}$ completely. Inverting the Fourier transform in (67), we obtain the real-space characterization

$$\bar{P}(x) = \int_0^\infty \frac{1}{(2\pi\sigma^2)^{1/2}}\, e^{-x^2/2\sigma^2} f(\sigma^2)\,d\sigma^2 \tag{68}$$

where $f(\sigma^2)$ is the probability density of the random variable

$$\sigma^2 = \frac{a\bar{U}^2}{(2D_\perp^*)^{1/2}}\int_0^1\int_0^1 \delta[\beta(s)-\beta(s')]\,ds\,ds' \tag{69}$$

Thus $\bar{P}(x)$ is a mixture, or "packet," of Gaussians. The dispersion of this packet is due to the large sample-to-sample fluctuations in the horizontal velocity component $U_1(y)$. The probability $\bar{P}(x)$ is analogous to the one found by Avellaneda and Majda[8,9,16] and Zumofen *et al.*[17] for a class of advection-diffusion equations in a stratified random velocity. In particular, see ref. 17 for a study of the tails of the density $\bar{P}(x)$ for $|x| \gg 1$.

5. MONTE CARLO SIMULATIONS FOR $V \neq 0$

This section constitutes a central part of this study. We report the results of Monte Carlo simulations for several values of $\bar{V}_1/\bar{U}$ and $\bar{V}_2/\bar{U}$, done in both the subcritical and the supercritical cases and for various directions of the mean velocity, including in the vicinity of the two resonant regimes. In all calculations, we consider the dimensionless version of Eqs. (3), obtained by introducing the dimensionless variables (26). In these new variables, the equations of motion become

$$\begin{cases} \dfrac{dx'(t')}{dt'} = U_1'(y'(t')) + \bar{V}_1' \\ \dfrac{dy'(t')}{dt'} = U_2'(x'(t')) + \bar{V}_2' \end{cases} \tag{70}$$

Here U_1' and U_2' have amplitudes ± 1, and the grid spacings are exponentially distributed with mean 1. A typical simulation procedure, for fixed values of $\bar{V}_1' = \bar{V}_1/\bar{U}$ and $\bar{V}_2' = \bar{V}_2/\bar{U}$, involves integrating (70), starting from $x'(0) = y'(0) = 0$, over 8192 independent, random realizations of the velocity $\mathbf{V}'(x', y')$ on squares of dimensions $\sim 2^{15}$, centered about (0, 0). This number of realizations corresponds to one quadrant of the Connection Machine 200 parallel computer, with each processor solving in parallel the equations over a separate realization. In other cross-velocity studies, we use $(8192)/4 = 2048$ processors for a given value of the mean velocity, so as to "process" four velocity points per run. The dimensionless time for which "thermalization," or dynamical equilibrium, is achieved is of the order $t'_{\max} \simeq 5 \times 10^3$. For such times, our choice of the box size is such that the Langrangian particles remain well within the dimensions of the boxes, without ever reaching the boundaries. This ensures that the statistics are well resolved by the computation with the aforementioned number of configurations, configuration size, and maximum dimensionless time. Error bars on the computed diffusivities are on the order of $\sigma = (2048)^{-1/2} = 0.03$. We note that the observed (typical) thermalization time is considerably shorter than the one found in other models of advection-diffusion in stratified fields, which can be as large as $t'_{\max} \cong 10^5$.[17] We believe that the shorter run times needed to resolve the fluctuations in our model are due to the random nature of the grid—as opposed to similar models based on a fixed regular grid, say, in which the velocity components take values $\pm \bar{U}$ randomly. The reason for this is that the exponential distribution simulates, in a coarse-grained sense, a "trend" of successive "layers" which have identical values for U_1 or U_2. The random barriers correspond to barrier locations at which trends are broken, and the present model avoids considering intermediate times at which the velocities remain unchanged. Of course, the "fixed" barrier model with random velocities and the present random barrier model with alternating velocities are in the same universality class as far as the long-time, large-scale properties are concerned (Section 2). We leave the discussion of computational aspects and algorithms to Section 6 and pass to the discussion of the results.

5.1. Mean Velocity Aligned with the Coordinate Directions

We consider first motions in which the mean velocity $\bar{\mathbf{V}}' = (\bar{V}_1', 0)$ is perfectly aligned with one of the coordinate directions (parallel-resonant case). This corresponds to $\bar{\mathbf{V}}'$ making an angle of 45°, 135°, 225°, or 315° with the fluctuating velocity in each random cell. The runs study the statistics of x' and y' for values of $\bar{V}_1' = n \times 0.125$, with $n = 1, 2, \ldots, 12$. First, we compute the Lagrangian history of $y'(t')$, $0 \leqslant t' \leqslant t'_{\max} = 5 \times 10^3$, and

consider the moments of $y'(t')$. Figures 7a, 8a, and 9a show the evolution in time of

$$\frac{1}{t'}\langle[y'(t')]^2\rangle_{nc}$$

in which $\langle\cdot\rangle_{nc}$ denotes averaging over noncycling trajectories in the subcritical case and $\langle\cdot\rangle_{nc}=\langle\cdot\rangle=$ usual averaging if $\bar{V}'_1\geqslant 1$. By definition, the computed transverse diffusivities are

$$D^*_\perp(\text{comp})=\frac{1}{2}\frac{1}{t'_{\max}}\langle[y'(t'_{\max})]^2\rangle_{nc}$$

They are shown in Table II. We also show the values of the product $\bar{V}'_1 D^*_\perp(\text{comp})$. The observed values of $\bar{V}'_1 D^*_\perp(\text{comp})$ are in excellent agreement with the exact result for $D^*_\perp$ in the supercritical case. We have also

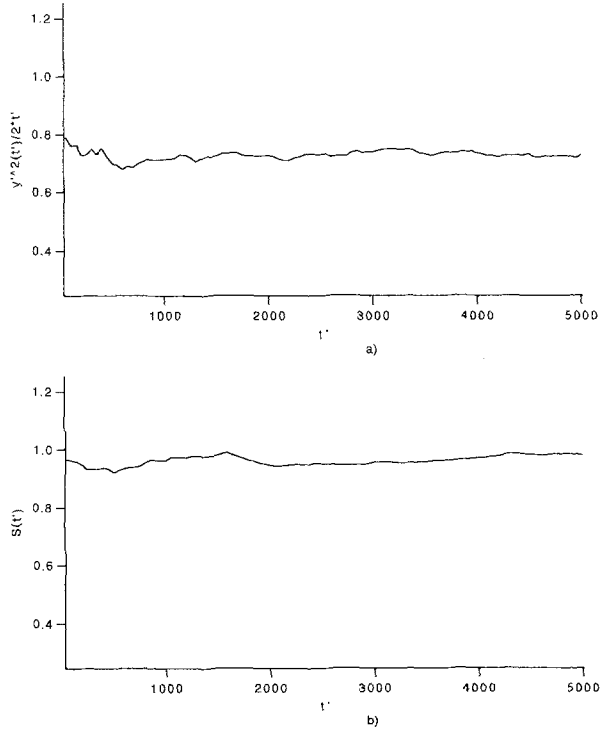

Fig. 7. Lagrangian history for the scaled mean-square displacements, with $\bar{V}'_1=\bar{V}_1/\bar{U}=0.5$ and $\bar{V}_2=0$. (a) Evolution of $\langle[y'(t')]^2\rangle/t'$; (b) evolution of $\langle[x'(t')-\langle x'(t')\rangle_{nc}]^2\rangle_{nc}$ $[2D^*_\perp(\text{comp})]^{1/2}/(t')^{3/2}$. The calculations are run for $t_{\max}=5\times 10^3$ dimensionless time steps.

computed, but not shown here, the *unconditional* second-order moments in the subcritical case

$$D_{\perp}^{*}(\text{uncond}) = \frac{1}{2}\frac{1}{t'_{\max}} \langle [y'(t'_{\max})]^2 \rangle$$

where the average is taken over *all* particles. We find that the relation

$$D_{\perp}^{*}(\text{uncond}) = p_{nc} D_{\perp}^{*}(\text{comp}) \tag{71}$$

holds for all velocities $\bar{V}'_1$ in the simulations. This means that *only the noncycling particles contribute to the transverse effective diffusivity at long times*. Relation (71) is not entirely obvious *a priori*, because closed streamlines can be arbitrarily large. In other words, the phase space splits into "cycling realizations," which can lead to arbitrarily long paths (with small probability), and "noncycling realizations," which occur with probability p_{nc}. The calculations show that the closed-streamline

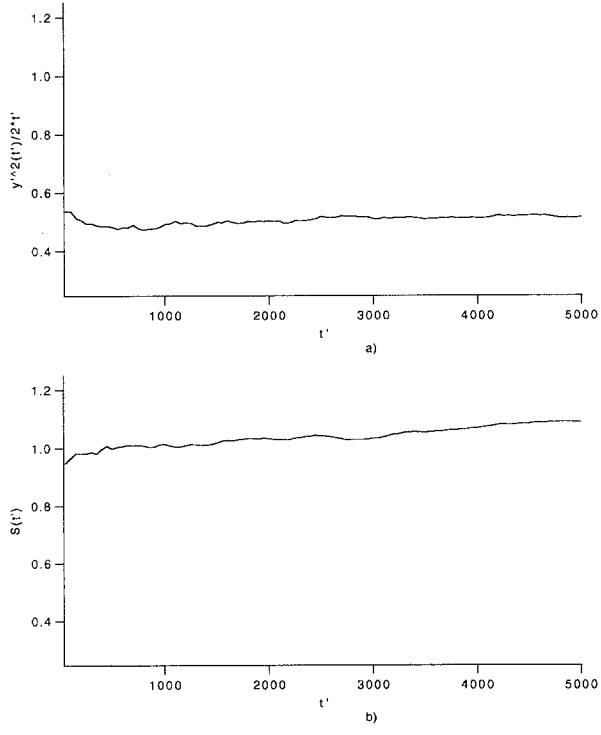

Fig. 8. Same as Fig. 7, with $\bar{V}'_1 = 1.0$ and $\bar{V}'_2 = 0$.

contribution to the long-time diffusivity is negligible, suggesting that the distribution of lengths of cycling particles for $\bar{V}'_1 \neq 0$ has very short tails. To test for Gaussianity of the transverse displacement, we compute the *flatness factors*

$$F_2(t') = \frac{\langle [y'(t')]^4 \rangle_{nc}}{\langle [y'(t')]^2 \rangle_{nc}^2}$$

(as before, $\langle \cdot \rangle_{nc} = \langle \cdot \rangle$ if $\bar{V}'_1 \geqslant 1$). The graphs of Lagrangian histories in Figs. 10a, 11a, and 12a show, unequivocally, a convergence of $F_2(t')$ to the Gaussian value of 3.0; see also Table IV. Finally, we evaluated the empirical probability densities of the rescaled values $y'(t'_{\max})/[2D^*_\perp(\text{comp})\, t'_{\max}]^{1/2}$. The histograms show very good agreement with the standard normal density $(2\pi)^{-1/2} \exp(-y^2/2)$ in all cases (Figs. 13a, 14a). We also computed, but do not display here, the empirical probability density functions by averaging over all particles (cycling and noncycling) for $y'(t'_{\max})/[2D^*_\perp(\text{uncond})\, t'_{\max}]$. The resulting curves are well fitted to Gaussians superposed with an additional strong peak at $y = 0$, reflecting

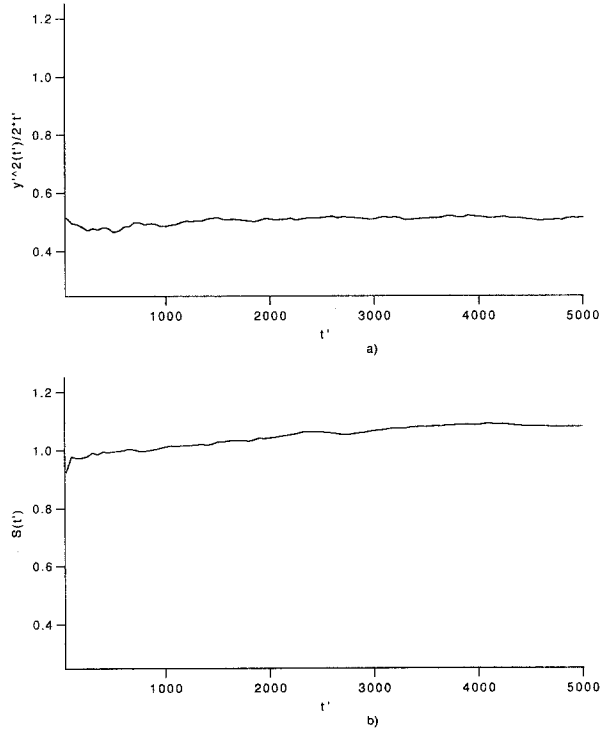

Fig. 9. Same as Fig. 7, with $\bar{V}'_1 = 1.5$ and $\bar{V}'_2 = 0$.

Table II. Computed (Dimensionless) Transverse Diffusivities in the Parallel-Resonant Case, with $0.125 \leqslant \bar{V}_1' \leqslant 1.5$ and $\bar{V}_2' = 0$[a]

$\bar{V}_1' = \bar{V}_1/\bar{U}$	$D_\perp^*(\text{comp})$	$\bar{V}_1' D_\perp^*(\text{comp})$
0.125	10.414	1.30175
0.250	4.01417	1.00354
0.375	2.18174	0.818153
0.500	1.45485	0.727425
0.625	1.07633	0.672706
0.750	0.815168	0.611376
0.875	0.667139	0.583747
1.000	0.515336	0.515336
1.125	0.460339	0.517881
1.250	0.411231	0.514039
1.375	0.372596	0.512319
1.500	0.342922	0.514383

[a] For $\bar{V}_1' \geqslant 1$, the dimensionless ratio $\bar{V}_1' D_\perp^*(\text{comp})$ $(= \bar{V}_1 D_\perp^*/a\bar{U}^2)$ agrees well with the value of 0.5 predicted by the theory. For $0 < \bar{V}_1' < 1$, this ratio increases as $\bar{V}_1'$ decreases.

the fact that the unconditional distribution for the y displacements is then a mixture of a Gaussian with diffusivity $D_\perp^*(\text{comp})$, occurring with probability p_{nc}, and of a Dirac mass at $y = 0$, occurring with probability $1 - p_{nc}$.

The x displacements were considered next. We considered the Lagrangian histories of the quantities

$$\frac{1}{(t')^{3/4}} [x'(t') - \langle x'(t) \rangle_{nc}]$$

averaging over the entire configuration space if $\bar{V}_1' \geqslant 1$ and over noncycling configurations if $\bar{V}_1' < 1$. The time histories of the normalized second moments

$$S(t') = \frac{[2D_\perp^*(\text{comp})]^{1/2}}{(t')^{3/2}} \langle [x'(t') - \langle x'(t') \rangle_{nc}]^2 \rangle_{nc}$$

were computed for $0 \leqslant t' \leqslant t'_{\max} = 5 \times 10^3$ (Figs. 7b, 8b, and 9b). The value of the scaling exponent $\nu = 3/2$ is confirmed accurately for all values of $\bar{V}_1'$.

In the supercritical cases and in subcritical regimes near $\bar{V}_1 = 1$, we obtain values of the scaled second moment

$$S_{\max} = \frac{[2D_{\perp}^{*}(\text{comp})]^{1/2}}{(t'_{\max})^{3/2}} \times \langle [x'(t'_{\max}) - \langle x'(t'_{\max}) \rangle_{nc}]^2 \rangle_{nc}$$

which are consistent with the prediction for the Matheron–de Marsily model [see Eq. (25)], which is $S_{\max} = 1.064$. The values of $S_{\max}$ are given in Table III. Notice that $S_{\max}$ decreases slightly as $\bar{V}'_1$ becomes less than 1 and then increases again as $\bar{V}'_1$ decreases further. These variations cannot be explained by the "uncoupled" Matheron–de Marsily model alone. They indicate that the notion of an "asymptotically independent" walker $y'(t')$ sampling weakly correlated horizontal layers with velocities ± 1 breaks

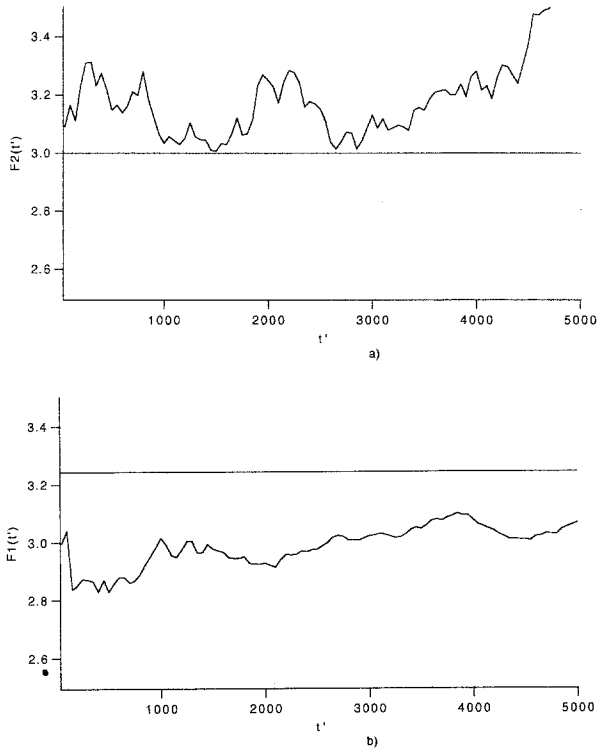

Fig. 10. Time evolution of the flatness coefficients: (a) $F_2(t')$, corresponding to diffusive transverse displacements; (b) $F_1(t')$, corresponding to superdiffusive longitudinal displacements. The dimensionless mean velocity is $\bar{V}'_1 = 0.5$, $\bar{V}'_2 = 0$.

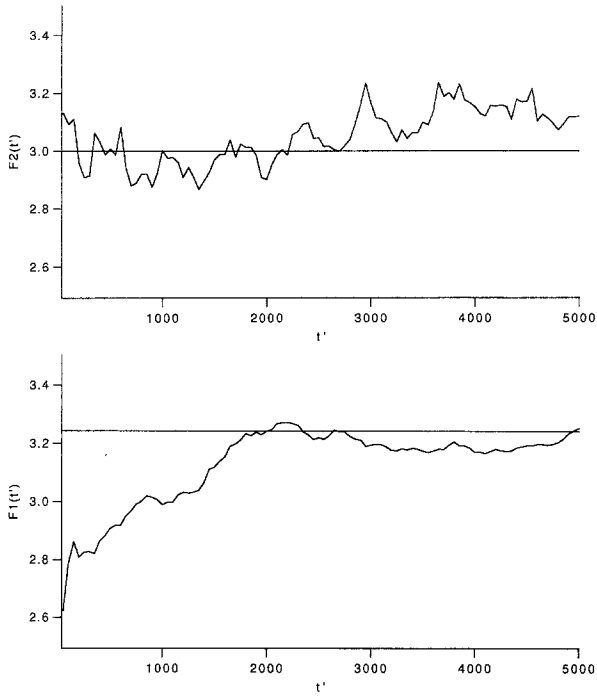

Fig. 11. Same as Fig. 10, with $\bar{V}'_1 = 1.0$ and $\bar{V}'_2 = 0$.

Table III. Scaled Mean-Square Displacements of the *x* Coordinate in the Parallel-Resonant Regime[a]

$\bar{V}'_1 (= \bar{V}_1/\bar{U})$	S_{max}
0.125	2.37642
0.250	1.38242
0.375	1.08846
0.500	0.977351
0.750	0.965704
0.875	1.01149
1.000	1.089
1.125	1.10411
1.250	1.08705
1.500	1.07994

[a] $\bar{\mathbf{V}} = (\bar{V}_1, 0)$, $S_{max} = \langle(\delta x)^2\rangle(2D^*_\perp)^{1/2}/(t'_{max})^{3/2}$. For $\bar{V}'_1 \geq 1$, the computed values agree reasonable well with the theoretical value $S_{max} = 1.06$. As $\bar{V}'_1$ decreases into the subcritical regime, S_{max} decreases and then increases again for small $\bar{V}'_1$ to $S_{max}(0.125) \simeq 2.37642$.

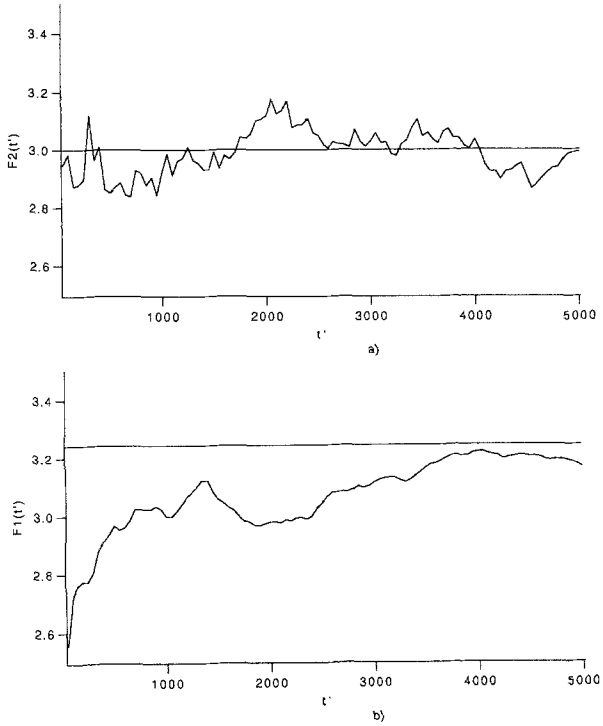

Fig. 12. Same as Fig. 10, with $\bar{V}'_1 = 1.5$ and $\bar{V}'_2 = 0$.

Table IV. Flatness Factors at the Largest Computed Time $t'_{max} = 5 \times 10^3$[a]

$\bar{V}'_1 (= \bar{V}_1/\bar{U})$	$F_1(t'_{max})$	$F_2(t'_{max})$
0.125	3.66729	3.44865
0.250	3.29743	3.35187
0.375	3.23094	3.2144
0.500	3.06737	3.51008
0.625	3.06871	3.0459
0.750	2.99027	2.93681
0.875	3.18939	3.06072
1.000	3.25388	3.11967
1.125	3.10637	3.06313
1.250	3.17016	3.023
1.375	3.17282	2.93768
1.500	3.16595	2.99158

[a] In the supercritical case, the computed values agree reasonably well with the predictions $F_1(t'_{max}) \cong 3.24$ (ref. 17) and $F_2(t'_{max}) = 3$. For subcritical velocities the computed values tend to increase as $\bar{V}'_1 \to 0$.

down as $\bar{V}_1'$ approaches 0, due to the increasingly stronger coupling between the x' and y' motions. The flatness factors

$$F_1(t') = \frac{\langle [x'(t') - \langle x'(t') \rangle_{nc}]^4 \rangle_{nc}}{\langle [x'(t') - \langle x'(t') \rangle_{nc}]^2 \rangle_{nc}^2}, \qquad t' = t'_{\max}$$

are computed in each case as well and are shown in Table IV. We find that, unless the mean velocity $\bar{V}_1'$ is very small, we obtain reasonable agreement with the asymptotic value of the Matheron–de Marsily model, $\lim_{t' \to \infty} F_1(t') = 3.24$, calculated by Zumofen *et al.*[17] For very small values of $\bar{V}_1'$ we find that $F_1(t'_{\max})$ exceeds the asymptotic value and is as large as 3.67, indicating that the tails of the distribution become longer. We also give plots of $F_1(t')$ as a function of time for a few values of the mean velocity in which the thermalization time is shown to be $t'_{\max} \sim 5 \times 10^3$ (Figs. 10b, 11b, and 12b).

Finally, the empirical density for scaled displacements in the x direction is shown in a few representative cases (Figs. 13b, 14b). In the sub-

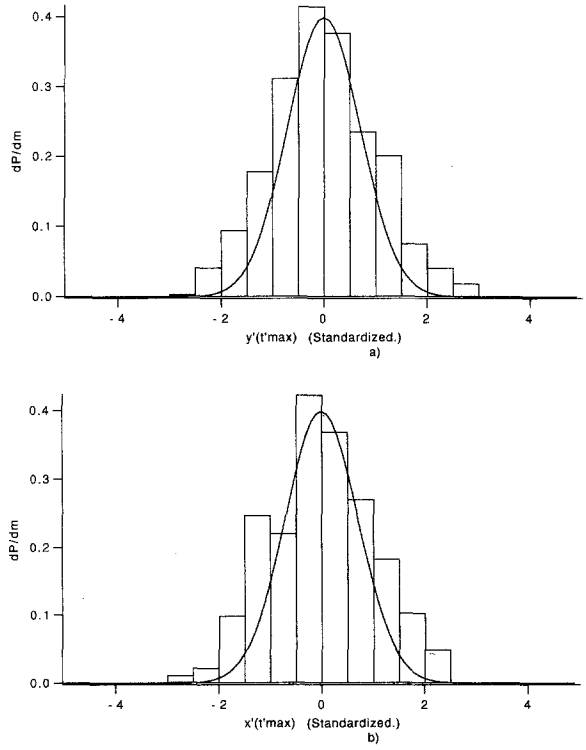

Fig. 13. Empirical probability distribution functions for $\bar{V}_1' = 0.5$, $\bar{V}_2' = 0$: (a) $y'(t'_{\max})/[2D_\perp^*(\text{comp})\, t'_{\max}]^{1/2}$; (b) $[x'(t'_{\max}) - \langle x'(t'_{\max}) nc]/(t'_{\max})^{3/4}$.

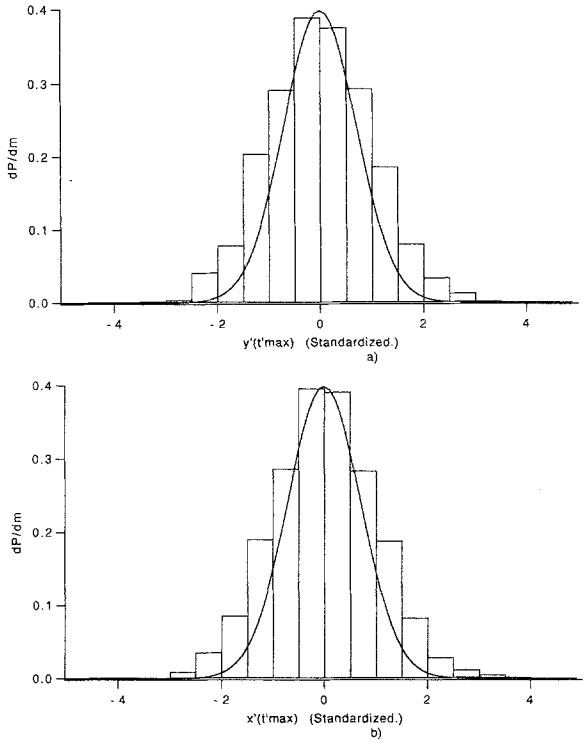

Fig. 14. Same as Fig. 13, with $\bar{V}'_1 = 1.5$ and $\bar{V}'_2 = 0$.

critical case, we computed the empirical densities unconditionally as well and found, as before, that the corresponding density is bimodal, with a strong peak at $x = 0$ corresponding to the fraction of trapped particles. In Figs. 13b and 14b only the conditional densities of $[1/(t')^{3/4}][x'(t') - \langle x'(t')\rangle_{nc}]$ are shown. This study confirms well that the basic mechanism for superdiffusion in the model in both the subcritical and supercritical cases is effectively described by the Matheron–de Marsily model of advection-diffusion in a stratified flow.

5.2. The Case $\bar{V}_1 \cdot \bar{V}_2 \neq 0$

We consider the general case when a nonzero mean velocity is not aligned with either coordinate direction. By symmetry, it suffices to study mean velocities such that $0 < \bar{V}'_2 \leqslant \bar{V}'_1$. In these regimes both coordinate processes are Fickian. When either component of the scaled mean velocity is greater than or equal to 1, we have shown that the diffusivities D^*_{11} and

D_{22}^* are given by formulas (24) and (24′). If both components of the dimensionless mean velocity are <1, the exact formulas are not expected to hold, although the processes are expected to be Gaussian.

We investigate the situation numerically by solving Langevin equations with scaled mean velocities $\bar{V}' = (p/4, q/4)$, for $1 \leqslant p \leqslant q \leqslant 6$ and for p and q not both 4, and with 2048 independent realizations per parameter set. These 20 groups of simulations are conducted for a dimensionless time $t'_{\max} = 5 \times 10^3$, by which thermalization has occurred. Table V illustrates that in the supercritical region the computed values of $\bar{V}'_2 D_{11}^*$ and $\bar{V}'_1 D_{22}^*$ agree very well with the analytical values. Table VI indicates that the flatnesses of the coordinate processes are also very close to 3, indicating a Gaussian distribution. Note that Table V shows that the measured values

Table V. Scaled Diffusivities for $\bar{V}_1 \cdot \bar{V}_2 \neq 0$[a]

$\bar{V}'_1$ $(= \bar{V}_1/\bar{U})$	$\bar{V}'_2$ $(= \bar{V}_2/\bar{U})$	$\bar{V}'_2 D_{11}^*$ (comp)	$\bar{V}'_1 D_{22}^*$ (comp)	$\bar{V}'_2 D_{11}^*$ [Eq. (24)]	$\bar{V}'_1 D_{22}^*$ [Eq. (24′)]
0.250	0.250	0.800782	0.75637	0.766667†	0.766667†
	0.500	0.757995	0.601123	0.690476†	0.880952†
	0.750	0.727046	0.692465	0.653846†	0.961538†
	1.000	0.615136	0.980242	0.633333	1.03333
	1.250	0.574151	0.94874	0.595238	0.97619
	1.500	0.564353	0.903717	0.572727	0.936364
0.500	0.500	0.70846	0.71973	0.833333†	0.833333†
	0.750	0.79158	0.75127	0.82†	0.98†
	1.000	0.82362	1.1239	0.833333	1.16667
	1.250	0.69864	1.03104	0.705128	1.01282
	1.500	0.641219	0.930725	0.642857	0.928571
0.750	0.750	0.869393	0.899385	1.07143†	1.07143†
	1.000	1.30803	1.60744	1.35714	1.64286
	1.250	0.812114	1.20876	0.887097	1.14516
	1.500	0.753819	0.973013	0.735294	0.970584
1.000	1.250	1.35353	1.55692	1.38889	1.61111
	1.500	0.842674	1.10022	0.9	1.1
1.250	1.250	0.928475	0.93629	0.944444	0.944444
	1.500	0.720294	0.835508	0.75974	0.811688
1.500	1.500	0.703318	0.704979	0.7	0.7

[a] Values are compared with the analytical formulas (24), (24′), which are valid only for $\rho = \max(\bar{V}'_1, \bar{V}'_2) \geqslant 1$. Comparison with the formulas is made in all cases. The predictions for subcritical velocities, for which agreement with (24), (24′) is not expected, are indicated with a dagger.

differ from the diffusivity formulas (24), (24′) in the subcritical regime. This is not surprising, due to the strong difference between the supercritical dynamics, which is essentially Markovian (Section 4), and the subcritical regime, in which the statistical structure of the paths is much more complex.

Finally, we consider the interesting "diagonal-resonant regime" $(\bar{V}'_1, \bar{V}'_2) \cong (1, 1)$. The formulas for diffusivity yield $D^*_{ii} = +\infty$ at the mean velocity $\bar{\mathbf{V}}' = (1, 1)$. To study the behavior near resonance, we consider sequences of mean velocities given by

$$\begin{pmatrix} \bar{V}'_1 \\ \bar{V}'_2 \end{pmatrix} = \begin{pmatrix} 1+\varepsilon \\ 1 \end{pmatrix} \tag{72}$$

and

$$\begin{pmatrix} \bar{V}'_1 \\ \bar{V}'_2 \end{pmatrix} = \begin{pmatrix} 1+\varepsilon \\ 1+\varepsilon \end{pmatrix} \tag{73}$$

Table VI. Flatness Factors at t'_{max} for $\bar{V}_1 \cdot \bar{V}_2 \neq 0$

$\bar{V}'_1$ $(= \bar{V}_1/\bar{U})$	$\bar{V}'_2$ $(= \bar{V}_2/\bar{U})$	$F_1(t'_{max})$	$F_2(t'_{max})$
0.250	0.250	3.17113	2.85691
	0.500	3.07298	2.97798
	0.750	2.99628	3.02925
	1.000	3.08793	3.09515
	1.250	3.05959	2.78072
	1.500	3.01326	3.0132
0.500	0.500	2.85941	2.83451
	0.750	2.85083	2.96737
	1.000	3.10962	3.08019
	1.250	2.87347	2.98388
	1.500	2.84699	2.97905
0.750	0.750	3.06965	3.30814
	1.000	2.94808	3.00763
	1.250	2.91541	2.8978
	1.500	3.03533	3.04495
1.000	1.250	2.98425	3.11788
	1.250	2.95214	2.90004
1.250	1.250	2.88694	2.97846
	1.500	2.90756	2.85447
1.500	1.500	3.02312	3.17572

with $\varepsilon = \pm 2^{-k}$, $6 \leqslant k \leqslant 9$. The "paths" (72) and (73) correspond to different approaches to the resonant value. On the basis of the exact formulas, we know that the divergence of D_{ii}^* depends on the path taken to (1, 1). The computations show that, for the path (72), we have

$$\bar{V}_1' D_{22}^* \cong \bar{V}_2' D_{11}^* \simeq \frac{0.25}{|\varepsilon|}, \qquad |\varepsilon| \ll 1 \tag{74}$$

which agrees with the explicit formulas in the supercritical region (Fig. 15a). [Note that the edges of the square bounding the subcritical region are supercritical ($\rho > 1$) and thus the exact formulas are expected to apply for ε positive and negative.] For the path (73), we find that, in the supercritical region ($\varepsilon > 0$), we have

$$\bar{V}_2' D_{11}^* = \bar{V}_1' D_{22}^* \cong \frac{0.125}{|\varepsilon|}, \qquad \varepsilon \ll 1 \tag{75}$$

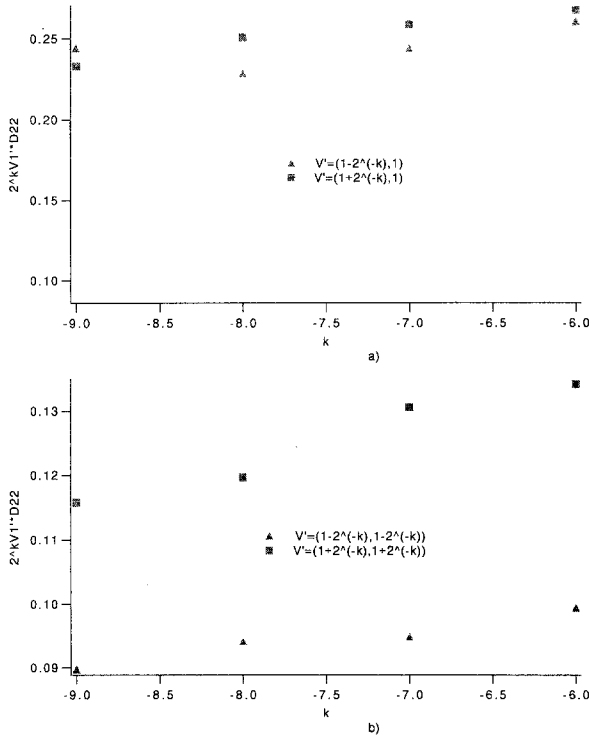

Fig. 15. Behavior of the effective diffusivities near diagonal resonance. (a) $2^{-k}\bar{V}_1' D_{22}^*$ plotted for $\bar{V}_2 = 1$ and (■) $\bar{V}_1' = 1 + 2^{-k}$, (▲) $\bar{V}_1' = 1 - 2^{-k}$. (b) $2^{-k}\bar{V}_1' D_{22}^*$ plotted for (■) $\bar{V}_1' = \bar{V}_2' = 1 + 2^{-k}$, (▲) $\bar{V}_1' = \bar{V}_2' = 1 - 2^{-k}$. Notice that in (b) the asymptotic coefficient is smaller as resonance is approached from the subcritical regime.

as predicted by (24), (57). On the other hand, approaching the diagonal resonance from the subcritical region ($\varepsilon < 0$) with the path (73) gives the different value

$$\bar{V}'_2 D^*_{11} = \bar{V}'_1 D^*_{22} \simeq \frac{0.1}{|\varepsilon|}, \qquad |\varepsilon| \ll 1, \tag{76}$$

(Fig. 15b). This shows again that the exact formulas (24), (24′) break down in the subcritical case.

6. COMPUTER SIMULATION OF THE RANDOM VELOCITY FIELD

We now describe the simulation of the random velocity constructed as a sum of two stratified orthogonal fields. For practical purposes, the computational domain is restricted to a square region of side $2L$. Several independent velocity fields can be generated from a single Poisson process on the line. Accordingly, consider $\{e_n\}$, a sequence of independent exponential random variables with mean 1. Such a sequence is produced by transforming an i.i.d. uniform sequence with the function $g(x) = -\log(x)$. Define $\{Z_n\}$ by $Z_n = \sum_{k=1}^{n} e_k$, and let $N(x) = \sup_k \{k \mid Z_k \leqslant x\}$. Then $N(\cdot)$ is a Poisson process and $\{Z_n\}$ is the sequence of jumps of this process. The barriers inside the computational "boxes" are sampled from the Poisson process $N(\cdot)$ as follows: first, consecutive intervals of length $2L$ of this process are assigned to each box, in order to represent the vertical random barriers $\{X_k\}$. Second, an additional sequence of consecutive segments of length $2L$ is generated and a segment is assigned to each box to represent the horizontal barriers $\{Y_l\}$. This sampling procedure is consistent with the assumption of statistical independence of $\{X_k\}$ and $\{X_l\}$ in each box and of statistical independence of different boxes.

6.1. The Algebra of Congruential Random Number Generators

A linear congruential generator (LCG) is used to generate the initial i.i.d. sequence of uniform random variables. The use of arithmetic random number generators is particularly well suited because, using the properties of the linear congruence, we minimize memory allocation (the environment is not *stored*, but instead *computed*). This is important in the simulations, given the memory storage available for each processor in the CM 200. A computation of this scale with direct storage would not be feasible.

To explain better the use of arithmetic in our simulation, we recall some algebraic properties of LCGs. An LCG is a map $f: S_m \to S_m$ defined

by $f(w) = (aw + c) \bmod m$, where $m > 1$ is an integer, $S_m = \{0, 1, ..., m-1\}$, $a, c \in S_m$, and a and m have greatest common divisor 1. The last condition is necessary and sufficient for f to be *invertible* (via Euclid's algorithm) so that f represents a permutation of S_m. Multiplication on the group of linear congruential generators modulo m is defined by

$$[a, c][d, f] = [(ad) \bmod m, (af + c) \bmod m]$$

for $[a, c] = ax + c \bmod m$ and $[d, f] = dx + f \bmod m$; this formula represents composition of LCGs. The identity is defined by $e = [1, 0]$. In particular, raising an LCG to a natural number power k can be done in $o(\log(k))$ operations by the recursive doubling formula $f^k = (f^{k \text{ div } 2})^2 * f^{k \bmod 2}$. This formula plays a pivotal role in initializing the positions of several particles independently and in parallel. The *order* of the LCG f as an element of the permutation group is defined as $\min\{s \mid f^s = e, s = 1, 2, ...\}$; Knuth[26] gives criteria for f to have maximal order.

We choose an LCG f with maximal order m ($= 2^{32}$ in our case). The LCG f represents a cyclic permutation where the sequences defined by $w_0 \in S_m$ and $w_n = f(w_{n-1})$ for $n > 0$ have a uniform distribution on S_m. Since f has inverse $f^{-1} = f^{m-1}$, we generate sequences in S_m with the formulas $w_0 = s$, $w_n = f(w_{n-1})$, and $w_n = f^{-1}(w_{n+1})$, where s is the seed. The sequence $\{Z_n \mid n = 0, 1, ...\}$ of jumps of the process $N(\cdot)$ is approximated by the formulas $Z_0 = 0$, $Z_n = Z_{n+1} - \log(w_n/m)$, and $Z_n = Z_{n-1} + \log(w_{n-1}/m)$. We represent the relative position of a particle with respect to the horizontal or vertical barriers as an ordered pair $(w_{N(x)}, x - w_{N(x)})$, the random integer and the offset from the previous jump, and use the recurrence relations for w_n and Z_n to compute relative motions. Each coordinate of the particle lies within an interval $[Z_n, Z_{n+1})$, for some n, between two jumps of the point process $N(\cdot)$.

6.2. Simulation of Particle Dynamics

We compute the dynamics of each particle using a simple discrete event simulation. The simulation consists of an intialization followed by a "strobe" loop.

During the initialization, each particle is positioned at the origin of its velocity field and its velocity is calculated as the sum of the mean velocity $\bar{\mathbf{V}}$ and the value of the $\bar{\mathbf{U}}$ field at the particle's position. The positioning process, which requires billions of logarithms and other floating point calculations, is carried out in parallel. For a sample of realizations of order 2K with $L = 2^{17}$, intialization requires only 5.33 cpu min. Moreover, the "random integer-offset" method of state representation makes it possible to

store the state of each particle in less than 1 Kbyte. Therefore, the initialization can be read from a file rather than calculated.

The strobe loop allows the dynamics of each particle to be simulated with only periodic synchronization of the collection of particles. At the beginning of the loop, a strobe time s is set equal to the current time for each particle. Next, the strobe time is incremented by one strobe period ds. Then, under the control of the event loop, each particle progresses randomly from one event to the next until it reaches the strobe time. Once all particles have reached the strobe time, the statistics for each group of particles are calculated. If the strobe time is not equal to the final strobe value, the process is repeated.

The event loop repeats a series of computations in parallel until each particle reaches the strobe time. First, the difference dt between the particle time t and the next strobe time s is calculated. Second, dt is compared to the times at which the particle would encounter the next change in sign in each shear field and to the time at which the particle would return to the origin if it moved at the current velocity. Then, dt is set to the minimum of these. If dt is equal to the return time, then the particle is marked as cyclic and its cycle period τ is recorded. The particle flows for the time dt at the current velocity, the new velocity and time are calculated, and the loop is repeated as necessary.

It becomes necessary to make an exception to the above sheme in the case of certain cyclic particles. When the cycle period of a particle is shorter than a single strobe period, the time of that particle is advanced for the maximum number of cycle periods less than a strobe period ds. This cycle optimization greatly improves the running time of the program in regimes where cycling occurs while maintaining the accuracy of the particle states at the strobe times. In all parameter regimes, 5000 time unit simulations with four groups of 2K independent particles require between 10 and 15 cpu min. (This usually translates to less than 30 min real time because the small memory and running time requirements of our simulation give it a high priority in job scheduling.) After the final strobe time, the current state of the particle array is saved. This allows probability distribution functions to be computed and, if necessary, to resume the calculation for longer times.

One future improvement of this simulation would be to sum several shear fields of varying amplitudes, length scales, and directions to simulate more general velocity fields corresponding to the Hamiltonians (5). This would be possible in the current scheme because the addition of each shear field (i.e., of an additional parallel array of random barriers) adds fewer than 100 bytes to the memory requirement per particle.

7. COMPARISONS WITH THE ISICHENKO–KALDA THEORY, DIA, AND CONCLUSIONS

7.1. Comparison with the Isichenko–Kalda Theory

Isichenko and Kalda (IK)[13] proposed a general theory for calculating box-exit probabilities and the fractal dimension of levels of a random Hamiltonian—the "statistical topography"—based on the analogy between level sets of random Hamiltonians and the hulls of percolation clusters. The IK theory concerns both *monoscale* Hamiltonians, which are stationary functions (i.e., statistically translation invariant), and hence characterized by a typical amplitude $\bar{H}$ and correlation length a, as well as *multiscale* Hamiltonians, which are nonstationary functions, characterized by a growth exponent h:

$$\langle |H(x, y)| \rangle \propto \bar{H} \left(\left| \frac{x}{z} \right| + \left| \frac{y}{a} \right| \right)^h, \qquad \left| \frac{x}{a} \right|, \left| \frac{y}{a} \right| \gg 1$$

In the case of monoscale Hamiltonians, Isichenko *et al.*[12] proved the existence of a critical level, based on a "flooding" topological argument. Using an analogy with percolation clusters near threshold, they derived the scaling relations

$$p_{nc}(L) \propto (L/a)^{-\alpha}$$

$$\langle \lambda(L) \rangle \propto (L/a)^{\gamma}$$

with

$$\alpha = 1$$

$$\gamma = 1 + \frac{1}{\nu} = \frac{7}{4}$$

Here ν is the exponent characterizing the divergence of the cluster diameter ξ near percolation. The value $\nu = 4/3$ is believed to be the exact exponent for 2D percolation based on conformal field theory; see Saleur and Duplantier.[28] The error bars for ν reported in the literature are $\sigma_\nu \approx 0.02$ (see ref. 29 and references cited in ref. 28).

For *multiscale* Hamiltonians, corresponding to $h > 0$, the situation is different. Isichenko and Kalda[13] used an interesting argument based on separation of scales to derive the exponents α and γ, which now depend on h as well as ν. The IK formulas for these exponents are

$$\alpha(h) = (1 - h) \frac{\nu}{1 + \nu}$$

$$\gamma(h) = 1 + \frac{1 - h}{1 + \nu}$$

In our model, we have $h = 1/2$ (Section 2), which corresponds to

$$\alpha(1/2) = 0.2857$$

and

$$\gamma(1/2) = 1.2143$$

exactly, if we take $\nu = 4/3$ and with errors $\sigma_\alpha = \sigma_\gamma < 0.02$ if the numerical uncertainty in the exponent ν of ref. 29 is taken into account. Comparing this with our computed values, $\alpha = 0.21 \pm 0.017$ and $\gamma = 1.28 \pm 0.015$, we find a discrepancy with the theoretical exponents of the order of at least 5%. This notwithstanding, the agreement with IK theory is rather good.

If we set aside the possibility of statistical error as a source for the discrepancy between the computed and the theoretical values, then a theoretical explanation must be sought. We believe that one reason for the difference is that the multiscale Hamiltonian H_0 has no critical level and its statistical topography is quite different from that of monoscale Hamiltonians. This suggests that the analogy with correlated percolation theory—the paradigm behind IK theory for $\alpha(h)$ and $\gamma(h)$—breaks down. It is also possible that the discrepancy is due to higher-order corrections to the values of α and γ obtained by the so-called scale-separation argument (ref. 15, §III.4).

7.2. Comparison with Mean-Field Theories for Effective Diffusivities

Consider the equations of motion in the integral form

$$x(t) - \bar{V}_1 t = \int_0^t U_1(y(s))\, ds \tag{77}$$

$$y(t) - \bar{V}_2 t = \int_0^t U_2(x(s))\, ds \tag{78}$$

The Kubo, or weak-coupling, approximations for D_{ii}^*, $i = 1, 2$, are obtained by replacing in the right-hand side of (77) and (78) the particle position $(x(s), y(s))$ by its mean position, $(\bar{V}_1 s, \bar{V}_2 s)$. This corresponds to second-order perturbation theory for D_{ii}^* in the parameter $\bar{U}$.[18,19] The corresponding approximate diffusivities are

$$D_{ii}^*(\text{Kubo}) = \int_0^\infty \langle U_i(\bar{V}_j s)\, U_i(0) \rangle\, ds, \qquad i \neq j, \quad i, j = 1, 2 \tag{79}$$

Using the explicit formulas for the velocity autocorrelation in (79) to compute the integral, we obtain

$$D_{ii}^*(\text{Kubo}) = \frac{a\bar{U}^2}{2\,|\bar{V}_j|}$$

This weak coupling approximation is exact *if one set of layers is removed*, e.g., D_{11}^* (Kubo) = the diffusivity corresponding to the velocity $\mathbf{V}(x, y) = (\bar{V}_1 + U_1(y), \bar{V}_2)$.

The direct interaction approximation (DIA) accounts for order-1 velocity fluctuations using a mean-field approach. Here, we derive the DIA for the model in Lagrangian variables; see ref. 3 for a similar treatment, and refs. 2 and 6. Accordingly, assume that the particle position in the right-hand side of (77)–(78) takes the form

$$x(s) = \bar{V}_1 s + [2D_{11}^*(\text{DIA})]^{1/2}\,\beta_1(s) \tag{80}$$

and

$$y(s) = \bar{V}_2 s + [2D_{22}^*(\text{DIA})]^{1/2}\,\beta_2(s) \tag{81}$$

where $D_{11}^*(\text{DIA})$ and $D_{22}^*(\text{DIA})$ are undetermined effective diffusivities, accounting for coherent effects of velocity fluctuations, and $\beta_i(t)$, $i = 1, 2$, are Brownian paths which are independent of $\mathbf{U}(x, y)$. Substituting (80)–(81) in (77)–(78), we can compute the large-time mean-square displacements $\langle [x(t) - \bar{V}_1(t)]^2 \rangle$ and $\langle [y(t) - \bar{V}_2(t)]^2 \rangle$. In this way, the following algebraic equations for $D_{ii}^*(\text{DIA})$ are found:

$$D_{11}^*(\text{DIA}) = \frac{a\bar{U}^2}{2\,|\bar{V}_2|}\left[1 + \frac{1}{1 + a\,|\bar{V}_2|/D_{22}^*(\text{DIA})}\right]$$

and

$$D_{22}^*(\text{DIA}) = \frac{a\bar{U}^2}{2\,|\bar{V}_1|}\left[1 + \frac{1}{a\,|\bar{V}_1|/D_{11}^*(\text{DIA})}\right] \tag{82}$$

These equations can be reduced to a single equation for the dimensionless quantity

$$\delta = \frac{|\bar{V}_i|\, D_{jj}^*(\text{DIA})}{a\bar{U}^2}, \qquad i, j = 1 \text{ or } 2, \quad j \neq i \tag{83}$$

namely,

$$\delta = \frac{1}{2}\left(1 + \frac{1}{1 + w/\delta}\right)$$

or

$$2\delta^2 + 2(w-1)\,\delta - w = 0 \tag{84}$$

where

$$w = \frac{|\bar{V}_1 \bar{V}_2|}{\bar{U}^2}$$

The positive solution of Eq. (84) is

$$\begin{aligned}\delta &= \frac{1}{2}\left[1 + (w^2+1)^{1/2} - w\right] \\ &= \frac{1}{2}\left[1 + \frac{1}{w + (w^2+1)^{1/2}}\right]\end{aligned} \tag{85}$$

Substituting for w and δ, we obtain

$$D_{ii}^*(\mathrm{DIA}) = \frac{a\bar{U}^2}{2\,|\bar{V}_j|}\left[1 + \frac{\bar{U}^2}{|\bar{V}_1 \bar{V}_2| + (\bar{U}^4 + \bar{V}_1^2 \bar{V}_2^2)^{1/2}}\right], \qquad i, j = 1, 2, \quad i \neq j \tag{86}$$

In particular, the theory predicts that

$$|\bar{V}_1|\, D_{22}^*(\mathrm{DIA}) = |\bar{V}_2|\, D_{11}^*(\mathrm{DIA}) \tag{87}$$

and

$$D_{ii}^*(\mathrm{DIA}) > D_{ii}^*(\mathrm{Kubo}) \tag{88}$$

In the supercritical case, we can compare these approximations with the exact formula

$$D_{ii}^* = \frac{a\bar{U}^2}{2\,|\bar{V}_j|}\left(1 + \frac{|\bar{V}_i|\,\bar{U}^2}{|\bar{V}_i| \cdot |\bar{V}_j^2 - \bar{U}^2| + |\bar{V}_j| \cdot |\bar{V}_i^2 - \bar{U}^2|}\right) \tag{89}$$

Clearly, $D_{ii}^* > D_{ii}^*(\mathrm{Kubo})$ for $\bar{V}_1 \bar{V}_2 \neq 0$. As $\bar{V}_1 \to 0$ or $\bar{V}_2 \to 0$, the corresponding transverse diffusivity converges to the Kubo value and the longitudinal diffusivity diverges. Therefore, the DIA accounts qualitatively for the enhancement of diffusivity due to fluctuations. Note, however, that the true diffusivities do not satisfy (87). Moreover, as $\bar{V}_1 \to 0$, $D_{22}^*(\mathrm{DIA}) \to 2D_{22}^*(\mathrm{Kubo})$ and hence the DIA does not predict the correct transverse diffusivity $[= D_{22}^*(\mathrm{Kubo})]$ near parallel resonance.

Table VII. Comparison of the Computed Dimensionless Diffusivities Scaled by the Dimensionless Velocities and the DIA[a]

$\bar{V}'_1$	$\bar{V}'_2$	$\bar{V}'_2 D^*_{11}$ (comp)	$\bar{V}'_1 D^*_{22}$ (comp)	$\bar{V}'_j D^*_{ii}$ (DIA)
0.000	0.125	1.30175	—	1
	0.250	1.00354	—	1
	0.375	0.818153	—	1
	0.500	0.727425	—	1
	0.625	0.672706	—	1
	0.750	0.611376	—	1
	0.875	0.583737	—	1
	1.000	0.515336	—	1
	1.125	0.517881	—	1
	1.250	0.514039	—	1
	1.375	0.512319	—	1
	1.500	0.514383	—	1
0.250	0.250	0.800782	0.75635	0.969726
	0.500	0.757995	0.601123	0.941391
	0.750	0.727046	0.692465	0.914963
	1.000	0.615136	0.980242	0.890388
	1.250	0.574151	0.94874	0.867595
	1.500	0.564353	0.903717	0.8465
0.500	0.500	0.70846	0.71973	0.840388
	0.750	0.79158	0.75127	0.8465
	1.000	0.82362	1.1239	0.809017
	1.250	0.69864	1.03104	0.777124
	1.500	0.641219	0.930725	0.75
0.750	0.750	0.869393	0.899385	0.792424
	1.000	1.30803	1.60744	0.75
	1.250	0.812114	1.20876	0.716616
	1.500	0.753819	0.973013	0.6901
1.000	1.250	1.35353	1.55692	0.675391
	1.500	0.842674	1.10022	0.651388
1.250	1.250	0.928475	0.93639	0.046301
	1.500	0.720294	0.835508	0.625
1500	1500	0.703318	0.704979	0.606107

[a] In the parallel-resonant case, dashes indicate an infinite longitudinal diffusivity and the DIA prediction applies only to the value of $\bar{V}'_2 D^*_{11}$(comp). Note: Values are taken from Tables II and V and we exchanged the indices in the values from Table II for better comparison.

As $(|\bar{V}_1|, |\bar{V}_2|) \to (\bar{U}, \bar{U})$ (diagonal resonance) the effective diffusivities diverge. The DIA, on the other hand, remains bounded near diagonal resonance and satisfies

$$D_{ii}^*(\text{DIA}) \simeq D_{ii}^*(\text{Kubo}) \times \frac{2+\sqrt{2}}{1+\sqrt{2}} \cong (0.72) \times a\bar{U}$$

The sharp increase in the actual diffusivity [Eqs. (74), (75)] is not accounted for by the mean-field approximation. In Table VII we compare $D_{ii}^*(\text{DIA})$ and D_{ii}^* for several values of $\bar{V}_1$, $\bar{V}_2$ in the supercritical region.

Finally, an assessment of the predictions of the DIA in the subcritical region can be made. We consider the dimensionless ratios $2r_{ii} = \bar{V}_j' D_{ii}^{*'} = \bar{V}_j D_{ii}^*/a\bar{U}^2$, where D_{ii}^* = actual diffusivity, or = DIA. The results are presented in Table VII. They show that the DIA does not perform well near the diagonal and parallel resonances. The agreement is better away from resonances, especially for $\bar{V}_1' \approx \bar{V}_2'$, which is not so surprising, given that the approximation implies $r_{11} = r_{22}$ [Eq. (87)], which is expected to be true only if $\bar{V}_1 = \bar{V}_2$ [Eq. (86)]. Table VII shows that the DIA approximation can take values both above or below the true diffusivities, according to the values of $\bar{\mathbf{V}}$. We can summarize the above analysis by saying that *a coherent, or self-consistent approximation, which takes into account velocity fluctuations through low-order correlation functions (e.g., two-point statistics), cannot account for the influence of the streamline topology* (stagnation, trapping, anomalous diffusion) *on the effective transport coefficients unless* $|\bar{\mathbf{V}}| \gg \bar{\mathbf{U}}$.

7.3. Conclusions

We constructed and analyzed a model for advection of particles by a random, incompressible velocity field. In this model, the Hamiltonian is not stationary, but instead has Brownian fluctuations, i.e., $\langle |H_0(x, y)|^2 \rangle \sim (|x| + |y|)$. Moreover, to analyze the influence of streamline topology on the transport, we neglected molecular diffusion. The particles were driven by a uniform drift.

For the case $\bar{\mathbf{V}} = 0$, the problem reduces to the study of the isolines of the random Hamiltonian H_0. We computed the statistics of percolating streamlines, both exit probabilities and fractal dimensions. Agreement with the theoretical exponents predicted by Isichenko and Kalda based on percolation theory was found to be good, although a discrepancy of 5–6% exists, even if statistical errors are taken into account. We believe that this discrepancy is due to the assumption of a virtual separation of scales in the IK calculations. On a more fundamental level, we established that the

statistical topography of the random Hamiltonian H_0 is completely different from the topography of "monoscale" Hamiltonians, for which the correspondence of the transport problem with percolation theory is exact. In fact, we showed that *all* streamlines are closed (localized) because every such streamline is always enclosed within another one with a higher or lower value of H_0. We believe that this is a universal feature of multiscale Hamiltonians, which have growing rms amplitudes $\langle |H(\mathbf{r})|^2 \rangle^{1/2} \sim |\mathbf{r}|^h$, $|\mathbf{r}| \gg 1$.

For $\bar{\mathbf{V}} \neq 0$, there is a net motion of particles, but if $\rho < 1$, a fraction of streamlines is closed. This regime can only be studied by Monte Carlo simulation. If $\rho \geqslant 1$, the trajectories are all open and we computed explicitly the asymptotic diffusivities. We found that two interesting resonances occur: if $\bar{V}_1 \cdot \bar{V}_2 = 0$, then the longitudinal fluctuations are superdiffusive with exponent $\nu = 3/2$. This exponent can be related to the Matheron–de Marsily model of diffusion in a stratified medium. If $\bar{V}_1 \cdot \bar{V}_2 \neq 0$, the motion is diffusive in all directions, but for $|\bar{V}_1|, |\bar{V}_2| \approx \bar{U}$, the effective diffusivity becomes very large, due to partial "trapping" of particles in "slow" pockets. These particles linger at far distances from the overall mean position $\mathbf{V}t$, producing a wide dispersion. The "diagonal resonance" described here is not accounted for by the direct interaction approximation.

Monte Carlo simulations in the subcritical regime show that the above descriptions of particle transport remain approximately valid for $\rho < 1$ if one considers the statistics of noncycling particles only.

Finally, the question of whether these effects are model dependent or generic poses itself. Regarding the statistical topography, we believe that the absence of critical streamlines is generic in the class of multiscale Hamiltonians. The superdiffusive motion with exponent 3/2 is due to the stratified nature of the ongitudinal velocity component. However, the model supports the idea whereby if the mean velocity $\bar{\mathbf{V}}$ points in a direction along which the fluctuations have long-range correlations, then superdiffusion can arise. The blowup of the diffusivities near diagonal resonance is of generic nature, in the following sense: for systems in which the mean-to-fluctuations ratio is ≈ 1, the probability is that some "stagnation pockets" with weak velocities will form, while in other regions $\bar{\mathbf{V}}$ and $\mathbf{U}(\mathbf{r})$ will align. This disparity may give rise to "resonances" in the effective diffusivity as $|\bar{\mathbf{V}}|/\bar{\mathbf{U}}$ varies. One can expect this resonance to exist for a wide class of non-Gaussian flows.

APPENDIX A. PERCOLATION OF STREAMLINES

This appendix contains the mathematical proofs of Propositions 2 and 3 of Section 3.

Proof of Proposition 2. The Hamiltonian for the case $\bar{\mathbf{V}} = \mathbf{0}$ is

$$H_0(x, y) = W_1(y) - W_2(x)$$

where W_i are continuous-time random walks, normalized so that $W_i(0) = 0$, $i = 1, 2$. In the proof, it is convenient to write H_0 in the form

$$H_0(x, y) = W_1(y) + W_2'(x) \tag{A.1}$$

where $W_2'(x) = -W_2(x)$ is again a random walk with the same distribution. Henceforth, we use (A.1) for H_0 and drop the prime over the second function.

Let B_L be the square of side $2L$ centered about $(0, 0)$ and let ∂B_L denote its boundary. We claim that

$$\text{Prob}\{H_0(\tilde{x}, \tilde{y}) < -2 \text{ for all } (\tilde{x}, \tilde{y}) \in \partial B_L, \text{ for some } L\} = 1 \tag{A.2}$$

which is the statement of Proposition 2. To calculate this probability, we write the event in (A.2) (for a given L) explicitly in terms of the walks W_i

$$\begin{aligned}
&\text{(i)} && \max_{0 \leqslant y \leqslant L} W_1(y) + W_2(L) < -2 \\
&\text{(ii)} && \max_{-L \leqslant y \leqslant 0} W_1(y) + W_2(L) < -2 \\
&\text{(iii)} && \max_{0 \leqslant y \leqslant l} W_1(y) + W_2(-L) < -2 \\
&\text{(iv)} && \max_{-L \leqslant y \leqslant 0} W_1(y) + W_2(-L) < -2 \\
&\text{(v)} && W_1(L) + \max_{0 \leqslant x \leqslant L} W_2(x) < -2 \\
&\text{(vi)} && W_1(L) + \max_{-L \leqslant x \leqslant 0} W_2(x) < -2 \\
&\text{(vii)} && W_1(-L) + \max_{0 \leqslant x \leqslant L} W_2(x) < -2 \\
&\text{(viii)} && W_1(-L) + \max_{-L \leqslant x \leqslant 0} W_2(x) < -2
\end{aligned} \tag{A.3}$$

Conditions (i) and (ii) state that $H_0(\tilde{x}, \tilde{y}) < -2$ on the vertical side of the square $\tilde{x} = L$, $-L \leqslant \tilde{y} \leqslant L$, and the other six conditions correspond to the negativity of H_0 on the remaining sides. The reason for splitting the conditions of negativity for each side into two is that the paths $\{W_i(z), z \geqslant 0\}$

and $\{W_i(z), z \leqslant 0\}$ are independent. Let us define a four-dimensional random walk $\mathbf{B}(\tau) = [B_1(\tau), B_2(\tau), B_3(\tau), B_4(\tau)]$, for $\tau \geqslant 0$, by

$$\begin{cases} B_1(\tau) = W_1(\tau) \\ B_2(\tau) = W_1(-\tau) \\ B_3(\tau) = W_2(\tau) \\ B_4(\tau) = W_2(-\tau), \qquad \tau \geqslant 0 \end{cases}$$

The negativity of $H_0(x, y)$ on ∂B_L can be expressed as an event pertaining to the behavior of the four-dimensional "path" $\mathbf{B}(\tau)$ for $0 \leqslant \tau \leqslant L$. We take advantage of this as follows: let Q_R denote a "cube" in four-dimensional space, defined by the inequalities $[\mathbf{r} = (x_1, ..., x_4)]$

$$-2R < x_i < R - 2, \qquad 1 \leqslant i \leqslant 4$$

Let τ_R denote the first exit time of the walk $\mathbf{B}(\tau)$ from Q_R. The inequalities (i), (ii),..., (viii) will be satisfied with $L = \tau_R$ if the walk exists Q_R through the portion of the boundary Γ_R defined by

$$\Gamma_R = \{\mathbf{r} \in \partial Q_R \mid -2R < x_i \leqslant -R, 1 \leqslant i \leqslant 4\} \tag{A.4}$$

In fact, if the walker exits the box Q_R through Γ_R, then $\max_{0 \leqslant \tau \leqslant \tau_R} B_i(\tau) < R - 2$, and, from (A.4), we have

$$(R-2) + B_i(\tau_R) < -2, \qquad 1 \leqslant i \leqslant 4$$

for all i. This ensures that (i)–(viii) are satisfied for $L = \tau_R$. The contention of Proposition 2 is that, as the walk $\mathbf{B}(\tau)$ evolves, it must exit Q_R through Γ_R for some R. To see this, we observe that as $R \to \infty$, $R^{-1}\mathbf{B}(\tau R^2)$ converges in distribution to a four-dimensional, standard Brownian motion with variance $a\bar{U}^2$ (see Section 2). Therefore, the conditional probability

$$p_R \equiv \text{Prob}\{\mathbf{B}(\tau_{2R}) \in \Gamma_{2R} \mid \mathbf{B}(\tau_R) \notin \Gamma_R\}$$

can be estimated, for $R \gg 1$, in terms of Brownian probabilities. More precisely,

$$p_R \approx \text{Prob}\{\beta(T_2) \in \tilde{\Gamma}_2 \mid \beta(T_1) \notin \tilde{\Gamma}_1\}, \qquad R \gg 1 \tag{A.5}$$

where T_1 is the first exit time of $\beta(\cdot)$ from the "box"

$$\tilde{Q}_1 = \{\mathbf{r}: -2 < x_i < 1, 1 \leqslant i \leqslant 4\}$$

and $\tilde{\Gamma}_1$ is the portion of the boundary of $\tilde{Q}_1$ defined by

$$\tilde{\Gamma}_1 = \{\mathbf{r} \in \partial Q_1 \mid -2 < x_i < -1\}$$

Similarly, in (A.5), T_2 is the first exit time from the box

$$\tilde{Q}_2 = \{\mathbf{r}: -4 < x_i < 2,\ 1 \leqslant i \leqslant 4\}$$

and $\tilde{\Gamma}_2$ is the portion of the boundary of $\tilde{Q}_2$ defined by

$$\tilde{\Gamma}_2 = \{\mathbf{r} \in \partial Q_1 \mid -4 < x_i < -2\}$$

Since $\tilde{Q}_1$ is contained in the interior of $\tilde{Q}_2$, by Harnack's principle (see, e.g., ref. 27), we have

$$\begin{aligned} &\text{Prob}\{\beta(T_2) \in \tilde{\Gamma}_2 \mid \beta(T_1) \notin \tilde{\Gamma}_1\} \\ &\quad \geqslant C\,\text{Prob}\{\beta(T_2) \in \tilde{\Gamma}_2 \mid \beta(0,0) = \mathbf{0}\} \end{aligned} \tag{A.6}$$

where C is a positive numerical constant. The probability on the right-hand side of (A.6) is strictly positive, since the surface area of $\tilde{\Gamma}_2$ is positive. All this shows that

$$\text{Prob}\{\mathbf{B}(\tau_{2R}) \in \Gamma_{2R} \mid B(\tau_R) \notin \Gamma_R\} > p, \qquad R \gg 1$$

for some fixed positive p, and hence

$$q_R \equiv 1 - p_R \equiv \text{Prob}\{\mathbf{B}(\tau_{2R}) \notin \Gamma_{2R} \mid \mathbf{B}(\tau_R) \notin \Gamma_R\} < 1 - p \tag{A.7}$$

for R large enough. Let

$$p_N = \text{Prob}\{B(\tau_{2^n}) \notin \Gamma_{2^n}, \text{ for } n < 1, 2, \ldots, N\}$$

Then, from (A.7),

$$\begin{aligned} p_N &= a_{2^{N-1}} \times q_{2^{N-2}} \times \cdots \times q_1 \\ &\leqslant \text{const} \times (1-p)^N \end{aligned}$$

Using this estimate, we calculate the probability that the Hamiltonian is $\geqslant -2$ on ∂B_L for all L. We have

$$\begin{aligned} &\text{Prob}\{H_0(\tilde{x}, \tilde{y}) \geqslant -2 \text{ for some } (\tilde{x}, \tilde{y}) \in \partial B_L, \text{ for all } L\} \\ &\quad \leqslant \text{Prob}\{H_0(\tilde{x}, \tilde{y}) \geqslant -2, \text{ for some } (\tilde{x}, \tilde{y}) \in \partial B_L, \\ &\qquad L = 2^N, \text{ for all integers } N\} \\ &\quad = \lim_{N \to \infty} p_N \\ &\quad \leqslant \lim_{N \to \infty} \text{const} \times (1-p)^N \\ &\quad = 0. \end{aligned}$$

This concludes the proof of Proposition 2. ■

Proposition 3 gives a quantitative estimate of the percolation probability for a box of size L, $L \gg 1$, in the form of the power law

$$p_{nc}(L) \leqslant CL^{-\alpha}, \qquad L \gg 1$$

where C is a constant and $\alpha > 0$. To obtain this result, we refine the proof of Proposition 2, taking advantage of the scaling relation

$$\tau_R \sim R^2$$

for the exit time of a Brownian motion from a box of size R.

Proof of Proposition 3. We have

$$\begin{aligned} &\text{Prob}\{|\mathbf{r}(t)| < L, \text{ for all } t\} \\ &\quad \geqslant \text{Prob}\{H_0 < -2, \text{ on } \partial B_l, \text{ for some } l \leqslant L\} \end{aligned}$$

Therefore,

$$\begin{aligned} p_{nc}(L) &\leqslant \text{Prob}\{H_0 \geqslant -2, \text{ somewhere on } \partial B_l, \text{ for all } l \leqslant L\} \\ &\leqq \text{Prob}\{\mathbf{B}(\tau_{2^n}) \notin \Gamma_{2^n}, \text{ for all } n = 1, 2, 3, \ldots, \\ &\qquad \text{such that } 2^n \leqslant L\} \end{aligned}$$

Set, accordingly,

$$E_N = \{\mathbf{B}(\tau_{2^n}) \notin \Gamma_{2^n}, \text{ for all } n \leqslant N\}$$

Then, for any positive integer N, we have

$$\begin{aligned} p_{nc}(L) &= \text{Prob}\{\text{streamline exits } B_L \text{ and } \tau_{2^N} \geqslant L\} \\ &\quad + \text{Prob}\{\text{streamline exists } B_L \text{ and } \tau_{2^N} < L\} \\ &\leqslant \text{Prob}\{\tau_{2^N} \geqslant L\} + \text{Prob}\{E_N\} \end{aligned} \tag{A.8}$$

The second probability was estimated in the proof of Proposition 2. To estimate the first term, observe that Q_{2^N} is contained in the hypersphere of radius $\rho_N = 2^{N+2}$ centered at $(0, 0, 0, 0)$. Hence,

$$\begin{aligned} \text{Prob}\{\tau_{2^N} \geqslant L\} &\leqslant \text{Prob}\{\sup_{\tau \leqslant L} |\mathbf{B}(\tau)| < \rho_N\} \\ &= \text{Prob}\{\sup_{\tau \leqslant L/\rho_N^2} |\rho_N^{-1}\mathbf{B}(\tau\rho_N^2)| < 1\} \end{aligned}$$

The stochastic process $\rho_N^{-1}\mathbf{B}(\tau\rho_N^2)$ has independent, identically distributed increments and converges in distribution to a homogeneous Brownian motion. Using this, it can be shown that

$$\text{Prob}\{\sup_{\tau \leqslant L/\rho_N^2} |\rho_N^{-1}\mathbf{B}(\tau\rho_N^2)| < 1\}$$

$$\leqslant e^{-C(L/\rho_N^2)}, \qquad \text{for} \quad \frac{L}{\rho_N^2} \gg 1 \tag{A.9}$$

where C is a constant independent of L and N. This inequality corresponds, formally, to the standard estimate for the exponential decay of probability that a Brownian path satisfies $\sup_{\tau < L/\rho_N^2} |\mathbf{B}(\tau)| < 1$ for $L/\rho_N^2 \gg 1$.[27] A justification of (A.9) using the theory of large deviations is given in Apelian.[21]

Putting together (A.8) and (A.9), we conclude that

$$p_{nc}(L) \leqslant \exp\left[-C_1\left(\frac{L}{2^{2N+4}}\right)\right] + C_2 \exp(-sN) \tag{A.10}$$

Here C_1 and C_2 are constants, and we used the estimate in the proof of Proposition 2

$$\text{Prob}(E_N) \leqslant C_2(1-p)^N \equiv C_2 e^{-sN}$$

i.e., we set $s = -\ln(1-p)$. We now choose N as a function of L, in the following fashion: Let γ be a fixed integer >2, and choose N such that

$$L = 2^{\gamma^N}$$

(Strictly speaking, this makes sense only for $L = 2^\nu$, but the case of general L is handled in the obvious way.) The choice $\gamma > 2$ ensures that $L/\rho_N^2 = L/2^{2N+4} \approx 2^{(\gamma-2)N}$ diverges as $N \to \infty$. Substituting $N = [1/(\gamma \log 2)] \log L$ in (A.10) gives

$$p_{nc}(L) \leqslant \exp[-C_1 L^{(1-2/\gamma)}] + C_2 L^{-s/(\gamma \log 2)}$$

The first summand is negligible compared with the last one for $L \gg 1$. Therefore, we conclude, as desired, that

$$p_{nc}(L) \leqslant CL^{-\alpha}, \qquad L \gg 1$$

where C is slightly larger than C_2 and $\alpha = s/\gamma \log 2$. ■

APPENDIX B. CALCULATION OF THE COVARIANCES $\langle \xi_1 \xi_j \rangle$ AND $\langle \eta_1 \eta_j \rangle$, $j \geqslant 1$, IN THE PROOF OF THEOREM 5

This appendix provides some complements to the proof of Theorem 5. Specifically, we derive the formulas for the autocorrelation functions ρ_w

and ρ_z [Eqs. (43), (44)] and using these functions, we compute the covariances $\{\xi_1 \xi_j\rangle$ and $\langle \eta_1 \eta_j\rangle$ for all $j \geqslant 1$.

B1. Autocorrelation Functions ρ_w and ρ_z

From the theory of stationary, two-state continuous-time Markov processes[22] we have the following result: if $\zeta(s)$ is such a process, with states ζ_+ and ζ_- and corresponding jump rates ρ_+ and ρ_-, then

$$\langle \zeta(s)\rangle = (\rho_+ \zeta_- + \rho_- \zeta_+)/(\rho_+ + \rho_-) \tag{B.1}$$

and

$$\langle \zeta(s)\,\zeta(s')\rangle = \langle \zeta(0)\rangle^2 + \frac{r_+ r_- (\zeta_+ - \zeta_-)^2}{(r_+ + r_-)^2} \exp[-(r_+ + r_-)\,|s-s'|] \tag{B.2}$$

In the case of the Markov process $w(s)$ introduced in Section 4,

$$\begin{aligned} \zeta_+ &= w_+ = 1/(\bar{V}_1 + 1) \\ \zeta_- &= w_- = 1/(\bar{V}_1 - 1) \\ \rho_+ &= r_+ = 1/(\bar{V}_1 + 1) \\ \rho_- &= r_- = 1/(\bar{V}_1 - 1) \end{aligned} \tag{B.3}$$

Substituting these values in (B.1) and (B.2), we find that

$$\langle w(s)\rangle = \frac{1}{\bar{V}_1}, \qquad s \geqslant 0 \tag{B.4}$$

and

$$\rho_w(s-s') = \langle w(s) - w(s')\rangle = \frac{1}{\bar{V}_1^2} + \frac{1}{\bar{V}_1^2(\bar{V}_1^2 - 1)} \times \exp\left(-\frac{2\bar{V}_1}{\bar{V}_1^2 - 1}\,|s-s'|\right)$$

The process

$$z(s) = 1 - \bar{V}_1 w(s)$$

can be analyzed using the above results. From (B.4),

$$\langle z(s)\rangle = 0, \qquad s \geqslant 0$$

and, since $z_+ = 1 - \bar{V}_1 w_+ = 1/(\bar{V}_1 + 1)$ and $z_- = 1 - \bar{V}_1 w_- = -1/(\bar{V}_1 - 1)$, using (B.2), we obtain

$$\langle z(s)\, z(s') \rangle = \frac{1}{\bar{V}_1^2 - 1} \exp\left(- \frac{2\bar{V}_1}{\bar{V}_1^2 - 1} |s - s'| \right)$$

B2. Evaluation of $\langle \xi_1 \xi_j \rangle$ and $\langle \eta_1 \eta_j \rangle$

At this point, we set

$$K = \frac{1}{\bar{V}_1^2(\bar{V}_1^2 - 1)}$$

$$Q = \frac{1}{\bar{V}_1^2 - 1}$$

and

$$R = \frac{2\bar{V}_1}{\bar{V}_1^2 - 1}$$

so that

$$\rho_w(s) = \frac{1}{\bar{V}_1^2} + K e^{-R|s|} \tag{B.5}$$

and

$$\rho_z(s) = Q e^{-R|s|} \tag{B.6}$$

We refer the reader to the formulas (45) and (46) for $\langle \xi_1^2 \rangle$ and $\langle \xi_1 \xi_j \rangle$. The integrals

$$\int_0^{p_1} \int_0^{p_1} \rho_z(\alpha(s - s'))\, ds\, ds'$$

and

$$\int_0^{q_1} \int_0^{q_1} \rho_z(\beta(s - s'))\, ds\, ds'$$

can be shown to be equal, by substituting formula (B.6) for ρ_z, to get

$$\frac{2Q}{R^2} (e^{-R\alpha p_1} - 1 + R\alpha p_1) \tag{B.7}$$

and

$$\frac{2Q}{R^2}(e^{-R\beta q_1} - 1 + R\beta q_1) \tag{B.8}$$

respectively.

Taking the expectation values of (B.7), (B.8) with respect to the exponential distribution, $\text{Prob}(p_1 > \tau) = e^{-\tau}$ and $\text{Prob}(q_1 > \tau) = e^{-\tau}$, we obtain the values

$$\frac{2Q}{1+R\alpha} \quad \text{and} \quad \frac{2Q}{1+R|\beta|} \tag{B.9}$$

respectively. The "mixed" terms

$$\int_0^{p_1}\int_0^{q_1} \rho_z(\alpha s - \beta s' - \alpha p_1)\, ds\, ds'$$

and

$$\int_0^{q_1}\int_0^{p_1} \rho_z(\beta s + \alpha p_1 - \alpha s')\, ds\, ds'$$

can be evaluated in a similar fashion. They are both equal to

$$Q\left(\frac{\alpha}{\alpha-\beta}\frac{1}{1+R\alpha} + \frac{\beta}{\beta-\alpha}\frac{1}{1+R|\beta|}\right) \tag{B.10}$$

Putting together (B.9) and (B.10), we obtain

$$\langle \xi_1^2 \rangle = \frac{2Q}{1+\alpha R} + \frac{2Q}{1+|\beta|R} + 2Q\left(\frac{\alpha}{\alpha-\beta}\frac{1}{1+R\alpha} + \frac{\beta}{\beta-\alpha}\frac{1}{1+R|\beta|}\right)$$

$$= 2Q\left(\frac{2\alpha-\beta}{\alpha-\beta}\frac{1}{1+R\alpha} + \frac{2\beta-\alpha}{\beta-\alpha}\frac{1}{1+R|\beta|}\right)$$

which is formula (47) of Section 4.

The calculation of $\langle \xi_1 \xi_n \rangle$ for $n \geqslant 2$ is best done in Fourier space, using the formula (B.6)

$$\rho_z(s) = Qe^{-R|s|}$$

$$= \frac{Q}{\pi}\int_{-\infty}^{+\infty} \frac{R}{R^2+k^2} e^{iks}\, dk$$

The integral

$$\int_0^{p_1}\int_0^{p_n} \rho_z(\alpha s + A_{n-1} - \alpha s')\, ds\, ds'$$

is therefore equal to

$$\frac{Q}{\pi}\int_{-\infty}^{+\infty} \frac{R\, dk}{R^2+k^2}\left[\int_0^{p_1}\int_0^{p_n} e^{ik(\alpha s + A_{n-1} - \alpha s')}\, ds\, ds'\right]$$

$$= \frac{Q}{\pi}\int_{-\infty}^{+\infty} \frac{R\, dk}{R^2+k^2}\left[\int_0^{p_1}\int_0^{p_n} e^{ik(\alpha s + \alpha s' + (A_{n-1} - \alpha p_1))}\, ds\, ds'\right]$$

In the last expression, we have made the change of variable $s' \leftrightarrow (p_1 - s')$ in order to exploit the independence of the exponential term $(A_{n-1} - \alpha p_1)$ and the limit of integration p_1. The expectation value of this quantity with respect to the exponential variables $\{p_j, q_j\}$ is readily computed because the double integral in brackets is equal to the product

$$\frac{e^{ik\alpha p_1} - 1}{ik\alpha}\frac{e^{ik\alpha p_n} - 1}{ik\alpha} \times e^{ik\beta q_1} \times e^{ik\alpha p_2} \times \cdots \times e^{ik\beta q_{n-1}}$$

Evaluation of the expectation leads to

$$\left\langle \int_0^{p_1}\int_0^{p_n} \rho_z(\alpha s + A_{n-1} - \alpha s')\, ds\, ds' \right\rangle$$

$$= \frac{Q}{\pi}\int_{-\infty}^{+\infty} \frac{R\, dk}{R^2+k^2}\frac{1}{(1+i\alpha k)^n (1+i\beta k)^{n-1}} \tag{B.11}$$

The remaining three integrals in (46) can be computed in a similar way. We find that

$$\left\langle \int_0^{p_1}\int_0^{q_n} \rho_z(\alpha s - \beta s' - A_{n-1} - \alpha p_n)\, ds\, ds' \right\rangle$$

$$= \frac{Q}{R}\int_{-\infty}^{+\infty} \frac{R\, dk}{R^2+k^2}\frac{1}{(1+i\alpha k)^n (1+i\beta k)^n} \tag{B.12}$$

$$\left\langle \int_0^{p_n}\int_0^{q_1} \rho_z(\alpha s + A_{n-1} - \beta s' - \alpha p_1)\, ds\, ds' \right\rangle$$

$$= \frac{Q}{\pi}\int_{-\infty}^{+\infty} \frac{R\, dk}{R^2+k^2}\frac{1}{(1+ik\alpha)^{n-1} (1+i\beta k)^{n-1}} \tag{B.13}$$

$$\left\langle \int_0^{q_1} \int_0^{q_n} \rho_z(\beta s + \alpha p_1 - \beta s' - A_{n-1} - \alpha p_n)\, ds\, ds' \right\rangle$$
$$= \frac{Q}{\pi} \int_{-\infty}^{+\infty} \frac{R\, dk}{R^2 + k^2} \frac{1}{(1 + ik\alpha)^{n-1} (1 + i\beta k)^{n-1}} \tag{B.14}$$

Adding together the integrals in (B.11)–(B.14) yields

$$\langle \xi_1 \xi_n \rangle = \frac{Q}{\pi} \int_{-\infty}^{+\infty} \frac{R\, dk}{R^2 + k^2} \frac{4 + 2i(\alpha + \beta) - \alpha\beta k^2}{(1 + i\alpha k)^n (1 + ik\beta)^n} \tag{B.15}$$

which is formula (48) in Section 4. The calculation of $\langle \eta_1 \eta_n \rangle$, $n \geqslant 1$, is similar, with slight differences. For brevity, we omit the details of the calculations leading to the final results,

$$\langle \eta_1^2 \rangle = \frac{1}{\bar{V}_1^2} + \frac{2k}{1 + \alpha R} + \frac{2K}{1 + |\beta|\, R}$$
$$- 2K \left(\frac{\alpha}{\alpha - \beta} \frac{1}{1 + R\alpha} + \frac{\beta}{\beta - \alpha} \frac{1}{1 + R\,|\beta|} \right)$$
$$= \frac{2}{\bar{V}_1^2} + 2K \left(\frac{\beta}{\beta - \alpha} \frac{1}{1 + R\alpha} + \frac{\alpha}{\alpha - \beta} \frac{1}{1 + R\,|\beta|} \right)$$

and

$$\langle \eta_1 \eta_n \rangle = \frac{R}{\pi} \int_{-\infty}^{+\infty} \frac{R\, dk}{R^2 + k^2} \frac{\alpha\beta k^2}{(1 + i\alpha k)^n (1 + i\beta k)^n}, \quad n \geqslant 2$$

B3. Explicit Evaluation of the Diffusivities D_{11}^* and D_{22}^*

From Section 4 and the preceding calculations, we find that

$$\langle \xi_1^2 \rangle + 2 \sum_{n=2}^{\infty} \langle \xi_1 \xi_n \rangle$$
$$= \langle \xi_1^2 \rangle + \lim_{N \to \infty} \sum_{n=2}^{N} \frac{2Q}{\pi} \int_{-\infty}^{+\infty} \frac{R\, dk}{R^2 + k^2} \frac{4 + 2i(\alpha + \beta)\, k - \alpha\beta k^2}{(1 + i\alpha k)^n (1 + i\beta k)^n}$$
$$= \langle \xi_1^2 \rangle + \frac{2Q}{\pi} \int_{-\infty}^{+\infty} \frac{R\, dk}{R^2 + k^2} \cdot$$
$$\times \frac{4 + 2i(\alpha + \beta)\, k - \alpha\beta k^2}{(1 + i\alpha k)(1 + i\beta k)[i(\alpha + \beta)\, k - \alpha\beta k^2]}$$

To evaluate the integral, which contains a denominator of order ik for $k \ll 1$, we split the domain of integration into $|k| \leqslant k_0$ and $|k| > k_0$, where k_0 is a small cutoff, and then pass to the limit as $k_0 \to 0$. In this way we find that

$$\begin{aligned}
&\frac{2Q}{\pi}\int_{-\infty}^{+\infty}\frac{R\,dk}{R^2+k^2}\,\frac{4+2i(\alpha+\beta)\,k-\alpha\beta k^2}{(1+i\alpha k)(1+i\beta k)[i(\alpha+\beta)\,k-\alpha\beta k^2]} \\
&\quad=\frac{2}{\bar V_1\cdot\bar V_2}+\lim_{k_0\to 0}\frac{2Q}{\pi}\int_{|k|\geqslant k_0}\frac{R\,dk}{R^2+k^2} \\
&\qquad\times\frac{4+2i(\alpha+\beta)\,k-\alpha\beta k^2}{(1+i\alpha k)(1+i\beta k)[i(\alpha+\beta)\,k-\alpha\beta k^2]} \\
&\quad=\frac{2}{\bar V_1\cdot\bar V_2}+\frac{2}{\bar V_1\bar V_2}\cdot\frac{\bar V_1}{\bar V_1|\bar V_2^2-1|+\bar V_2|\bar V_1^2-1|}
\end{aligned}\tag{B.16}$$

where the first term corresponds to the contribution from a neighborhood $|k| \leqslant k_0$, $k \ll 1$, and the second term is obtained by computing the integral by partial fraction expansion of the integrand and letting $k_0 \to 0$. Multiplying (B.16) by $1/(2\langle\tau_1\rangle) = \bar V_1/4$, we obtain the desired expression for D_{11}^* in dimensionless variables.

The calculation of

$$\begin{aligned}
&\langle\eta_1^2\rangle+2\sum_{n=2}^{\infty}\langle\eta_1\eta_n\rangle \\
&\quad=\langle\eta_1^2\rangle+\frac{2Q}{\pi}\int_{-\infty}^{+\infty}\frac{R\,dk}{R^2+k^2}\,\frac{\alpha\beta k^2}{(1+i\alpha k)(1+i\beta k)[i(\alpha+\beta)\,k-\alpha\beta k^2]}
\end{aligned}$$

is simpler because the integral is absolutely convergent and can be easily computed using the expansion for the integrand in partial fractions. The details of this straightforward, but tedious, computation are omitted.

ACKNOWLEDGMENTS

We thank M. B. Isichenko, A. J. Majda, G. C. Papanicolaou, K. Riedel, and E. B. Tatarinova as well as the referees for interesting discussions and constructive suggestions. A grant from the Army High-Performance Computing and Research Center (AHPCRC) for time on the CM 200 parallel computer is gratefully acknowledged. This research was partially supported by grants NSF-DMS-9207085 (National Science Foundation), ARO-DAAL-03-92-G0011 (U.S. Army), and AFOSR-90-0090 (U.S. Air Force).

REFERENCES

1. B. Yaron, G. Dagan, and J. Goldshmid, eds., *Pollutants in Porous Media* (Springer-Verlag, Berlin, 1984).
2. R. Kraichnan, *Phys. Fluids* **13**:22 (1970).
3. D. L. Koch and J. F. Brady, *Phys. Fluids A* **1**:49 (1989).
4. M. Avellaneda and A. J. Majda, *Phys. Rev. Lett.* **68**:3028 (1992).
5. R. Kraichnan, in *The Padé Approximant in Theoretical Physics*, G. A. Baker, Jr., and Gammel, eds. (Academic Press, New York, 1970) p. 129.
6. R. Kraichnan, *Complex Systems* **1**:805 (1987).
7. G. Matheron and G. de Marsily, *Water Resources Res.* **16**:910 (1980).
8. M. Avellaneda and A. J. Majda, *Commun. Math. Phys.* **131**:339 (1990).
9. M. Avellaneda and A. J. Majda, *Commun. Math. Phys.* **146**:139 (1992).
10. S. Redner, *Physica* **38D**:287 (1989).
11. J. P. Bouchaud, A. Georges, J. Koplik, A. Provata, and S. Redner, *Phys. Rev. Lett.* **64**:2503 (1990).
12. M. B. Isichenko, J. L. Kalda, E. B. Tatarinova, O. V. Telkovskaia, and V. V. Yankov, *Sov. Phys. JETP* **69**:517 (1989).
13. M. B. Isichenko and J. L. Kalda, *J. Nonlinear Sci.* **1**:3 (1991).
14. M. B. Isichenko and J. L. Kalda, *J. Nonlinear Sci.* **1**:375 (1991).
15. M. B. Isichenko, *Rev. Mod. Phys.* **64**:961 (1992).
16. M. Avellaneda and A. J. Majda, *J. Stat. Phys.* **69**:689 (1991).
17. R. Zumofen, J. Klafter, and A. Blumen, *J. Stat. Phys.* **65**:991 (1991).
18. R. Kubo, *J. Math. Phys.* **4**:174 (1963).
19. Q. Zhang, *J. Stat. Phys.* **66**:485 (1992).
20. A. M. Soward and S. Childress, *Phil. Trans. R. Soc. Lond. A* **331**:649 (1990).
21. C. Apelian, In preparation.
22. U. N. Baht, *Elements of Applied Stochastic Processes* (Wiley, New York, 1972).
23. H. Kesten and G. C. Papanicolaou, *Commun. Math. Phys.* **65**:19 (1979).
24. A. I. Ibragimov, *Theor. Prob. Appl.* **7**:349 (1962).
25. P. Billingsley, *Convergence of Probability Measures* (Wiley, New York, 1968).
26. D. E. Knuth, *The Art of Computer Programming*, Vol. II: *Seminumerical Algorithms* (Addison-Wesley, Reading, Massachusetts, 1973).
27. A. Friedman, *Stochastic Differential Equations and Applications* (Academic Press, New York, 1975).
28. H. Saleur and B. Duplantier, *Phys. Rev. Lett.* **58**(22):2325 (1987).
29. P. Grassberger, *J. Phys. A* **19**:2675 (1986).